JECE 2020-Santi

by Darma Santi

Submission date: 19-Apr-2023 04:59PM (UTC+0900)
Submission ID: 2069162276
File name: JECE_2020-Santi.pdf (3.28M)
Word count: 10391
Character count: 54359

Journal of Environmental Chemical Engineering 8 (2020) 103735

Contents lists available at ScienceDirect

Journal of Environmental Chemical Engineering

journal homepage: www.elsevier.com/locate/jece

Hydrocracking of pyrolyzed α-cellulose to hydrocarbon over M_xO_y/Mesoporous carbon catalyst (M = Co and Mo): Synthesis and characterization of carbon-based catalyst support from saw waste of Merbau wood

Darma Santi[a,b], Triyono[a,*], Wega Trisunaryanti[a], Iip Izul Falah[a]

[a] Department of Chemistry, Faculty of Mathematics and Natural Science, Universitas Gadjah Mada, Sekip Utara Bulaksumur, Yogyakarta, 55281, Indonesia
[b] Department of Chemistry, Faculty of Mathematics and Natural Science, Universitas Papua, Jl. Gunung Salju Amban, Manokwari, 98314, Indonesia

ARTICLE INFO

Keywords:
Hydrocracking
Hydrocarbons
Mesoporous
Merbau wood

ABSTRACT

Single-step synthesis of mesopore carbon (MC) was synthesized via carbonization and oxidation of saw waste of Merbau wood (Intsia, spp). MC as support M_xO_y (M = Co, and Mo, x and y represent the type of metal oxide formed) were synthesized and introduced to the hydrocracking of pyrolyzed α-cellulose (bio-oil). The MC samples were characterized by XRD, FT IR, total acids groups obtained titrimetry by Boehm method, SEM, and Surface Area Analyzer (SAA). The two highest specific surface area of the MC, which was carbonized at 800 °C for 3 h (MC83) and at 700 °C for 2 h (MC72), were 350.56 m^2/g and 330.31 m^2/g, respectively. The MC72 showed the highest average pore diameter of 2.758 nm. The MC72 was then used as a support of cobalt and molybdenum metal (Co/MC72 and Mo/MC72) as a catalyst hydrocracking of bio-oil. The SAA results showed that the specific surface area of Co/MC72 has increased to 384.7 m^2/g and of Mo/MC72 has decreased to 25.43 m^2/g. The results showed the Co/MC72 and Mo/MC72 catalyst improved the quantity (as conversion 75.33 and 74.69 wt.%, respectively) and quality of bio-oil (as selectivity toward hydrocarbon compound of analyses by Co/MC72 and Mo/MC72, moreover the alkenes by Co/MC72). The liquid product consisted of C_2-C_6 of aldehydes, ketones, acids, alcohols, furans, phenols, and hydrocarbons. The hydrocarbon compounds contained propane (11.56 wt%), 2-deutero-2-methyl propane (24.90 wt.%) and 4-methyl-1-pentene (1.11 wt%).

1. Introduction

The quest for alternative sources of energy from renewable carbon sources and meet the aspects of sustainability, one of them is from biomass sources, is still being carried out until now. The use of lignocellulosic materials is particularly safe and cost-effective, as the feedstock is not in competition with food. Cellulose is still the most widespread renewable carbon and has enormous potential for the development of valuable bio-based platform molecules as an alternative raw material. Therefore, increasing attention has been paid to converting cellulose into value-added fuels and chemicals. In this study, α-cellulose was used as a compound model in testing the catalytic activity of the synthesized catalyst material.

Bio-oil obtained as a liquefied form of cellulose, which converted through the pyrolysis process, still has shortages as fuels. Water and a wide range of oxygen-containing compounds are responsible for most bio-oil drawbacks, including low heating, corrosiveness, chemical, and thermal volatility, and fossil fuel immiscibility. One of the most common ways to enhance the quality of bio-oil is to reduce the oxygenated compounds by converting undesirable compounds (acids, aldehydes, ketones, esters, ethers, and others) into desirable compounds (hydrocarbons) [1]. The method of upgrading usually takes place in the presence of a catalyst, which requires one to improve the yield of less oxygenated compounds [1,2].

Before this, the synthesis of heterogeneous catalysts with different compositions and morphology has been extensively investigated for different applications. The research work in the field of green chemistry has been dedicated to the subject with special attention to fine chemical synthesis, such as MoS_2-PDA-Ag nanocomposites via a combination of mussel-inspired chemistry and microwave irradiation method as catalyst towards 4-nitrophenol reduction [3], mesoporous silicates for molecular sieves application using (Cs)Al-SBA-15 [4], zeolites for biodiesel production [5], catalytic cracking of waste chicken fat using coal fly ash [6] and application of carbon materials in hydrogenation

* Corresponding author.
E-mail address: triyn102@ugm.ac.id (Triyono).

https://doi.org/10.1016/j.jece.2020.103735
Received 1 January 2020; Received in revised form 14 January 2020; Accepted 1 February 2020
Available online 03 February 2020

reactions [7].

There are several published about the use of catalysts for upgrading efforts, which involve the use of zeolites [8–10], carbon [11], and mesoporous material [12]. Recently, mesoporous catalysts and their support systems are derived from synthetic materials such as MCM-41 [13,14], SBA-15 [15], and MSU [16] used to improve the large molecular oligomers for their ability. However, the success of catalyst support materials that come from nature has never been reported, especially those which are selective in hydrocarbon compounds.

Nevertheless, research was also reported on the application of metal oxides catalyst (NiO [8,17], MoO_2 [18], CoO, and Co_3O_4 [19]. NiO based catalysts are effectively to produce low oxygen content and adequate organic yield [8], but they become inactive by carbon deposition [20]. Furthermore, active metal sintering can also occur to reduce the catalytic stability. One possible solution for this drawback is the development of catalysts with strong metal support interactions and a suitable containment of metal particles, one of which involves a carbon-based support system. Therefore, this research used catalysts of active metal nanoparticles that are carried on carbon synthesized from Merbau wood. The advantages of this type of catalyst are involving the contribution of acid sites from metals and preventing agglomeration of metal because dispersing the transition metals to the porous system such as mesoporous carbon [15], mesoporous silica [21], and MCM-41 [22].

The techniques for processing an activated carbon involves two steps-pyrolysis and activation. In the pyrolysis step, the temperature of carbonization from 400 to 850 °C is often 1000 °C. In the activation proses, these chars as a result of the pyrolysis step activated in oxidizing gas such as air, carbon dioxide, or steam at a temperature of about 800–1000 °C to produce the final activated carbon. The use of high temperature [23] and these types of selected gas result activated carbon with high micropore. Furthermore, the active catalyst support required the large surface area that provides sufficient active sites for loading catalytic metal nanoparticles. Moreover, mesopore is required for adsorption purposes, diffusion, and accelerated transport [24,25]. The previous study revealed that the lower temperature, 350 °C with oxidized in the oxygen stream, produced the mesoporous activated carbon [26].

In this work, one of the studies was to evaluate the influence of carbonization temperatures and hold time of carbonization on characteristics porosity in carbonized Merbau wood. Different products can be selectively produced depending on the catalyst characteristics, while increased deoxygenation can generate bio-oil with improved physical and chemical properties. Furthermore, this research evaluates the catalytic performance of cobalt/carbon and molybdenum/carbon catalysts with hydrocracking, as a biomass model of pyrolyzed α-cellulose. This work is focused on developing selective catalysts to either transform the highly oxygenated compounds into hydrocarbons or reduce the formation of unwanted bio-oil components (e.g., acids, carbonyls, aldehydes).

2. Experimental

2.1. Material and methods

Merbau wood samples used as raw materials were obtained from Manokwari, Indonesia. The raw materials were shaped chips as saw waste and manually chosen, dried at 110 °C to remove any surface moisture. The schematic diagram of the apparatus for the preparation of activated carbon was shown in supplementary information as Fig. S1. KOH, NaOH, $NaHCO_3$, Na_2CO_3, $Co(NO_3)_2{\cdot}6H_2O$ (Merck), $(NH_4)_6Mo_7O_{24}{\cdot}4H_2O$ (Merck), acetone, HCl were analytical grade and obtained from Merck, α-cellulose was obtained from Sigma-Aldrich.

2.1.1. Carbonization of Merbau woods

Prior to carbonization, Merbau woods were ground to obtain a sample size of less than 2 mm. After that, Merbau woods were loaded on tubular stainless steel, which was inserted within a cylindrical stainless steel reactor with a 6 cm internal diameter. The Merbau woods were heated up to carbonization temperature (500, 600, 700 and 800 °C) at the heating rate 10 °C/min, and were held for each variation of hold time (1, 2, and 3 h) under N_2 gas at a flow rate of 20 mL/min. The samples were cooled below N_2 flow to room temperature.

2.1.2. Activation of the carbonized Merbau woods

All of the carbonized samples for each variation (temperature carbonization and hold time carbonization) were loaded on tubular stainless steel which placed inside a reactor as uses as a carbonization step. Subsequently, the tubular furnace then heated to 350 °C at a loading rate of 10 °C/min, under O_2 gas flow within flow rate 15 mL/min for 3 h. Mesopore carbon Merbau samples from this step (MC) that carbonized at 500 °C for 1, 2 and 3 h were noted MC51, MC52, MC53, at 600 °C were noted MC61, MC62, MC63, at 700 °C were noted MC71, MC72, MC73, at 800 °C were noted MC81, MC82, and MC83.

2.1.3. Catalysts preparation

MC72 was sieved with a 60–80 mesh and soaked with acetone at room temperature for 2 h, and then filtered. MC was then soaked with 1 M with the same preparation condition as the previous step, followed by thorough washing with deionized water and drying at 105 °C for 12 h.

MC72 was impregnated with cobalt by wetness impregnation technique. The amounts of metals used in the impregnation process were about 1.0 wt.%. $Co(NO_3)_2{\cdot}6H_2O$ salt was dissolved in deionized water. MC72 was inserted into the salt solution. The mixture was stirred for 2 h at 80 °C. The solid was dried at 90 °C for 7 h. The solid was then calcined at 500 °C under nitrogen gas stream with a flow rate of 20 mL/min for 4 h. The Mo metal impregnation is carried out using the same method as the Co metal. The final products were Co/MC72 and Mo/MC72 catalysts. Co/MC72, Mo/MC72 catalysts, and MC72 samples were measured acidity value by acidity test using the ammonia adsorption method.

2.1.4. Catalyst acidity test

The acidity value of the catalysts was measured by streaming the ammonia vapor onto the sample in a vacuum chamber for 24 h at room temperature. The acidity value (g/mol) of the catalysts was calculated using the following equation [26] with any modification the type of gas adsorbate using the ammonia vapor:

$$\text{Acidity value} = \frac{G - G_0}{G_0 \times M_r.\text{ammonia}} \quad (1)$$

Where G is the weight of samples after adsorption (g), G_0 is the weight of samples before adsorption (g), and M_r.ammonia is the molecular weight (g/mol).

2.1.5. Hydrocracking of α-Cellulose

The hydrocracking of α-cellulose was performed in a two-step. The first step was the pyrolysis of α-cellulose at 600 °C for 3 h with a nitrogen gas stream with a flow rate of 20 mL/min in a stainless steel semi-batch reactor. The second step was hydrocracking of α-cellulose pyrolysis oil, which was obtained from the first step using the catalysts at 450 °C for 2 h with hydrogen gas stream with a flow rate of 20 mL/min in a stainless steel semi-batch reactor (catalyst/feed ratio was about 1/30). The liquid products were analyzed using GC–MS.

2.2. Detection method

The functional groups as analysis surface chemistry of the samples were recorded between 4000 and 400 cm-1 using Fourier Transform Infrared Spectrometer (FTIR, Shimadzu Prestige-21) with KBr disc technique. Boehm titration was also extended to porous carbons to

evaluate acidic sites on the surface. Refer to this updated form, a sample of 1.5 g was applied to 50.00 mL of 0.05 M $NaHCO_3$, Na_2CO_3, and NaOH reaction base. A magnetic stirrer agitated the suspensions at room temperature for 24 h, filtered, and pipetted 10 mL of the filtrate and titrated with either 0.05 M HCl to calculate the amount of acidic site [27–29]. X-ray diffraction (XRD) pattern of activated carbon obtain from different conditions of preparation were recorded using a Rigaku Miniflex600, λ = 1,54 Å, 40 kV, 15 mA). The particle size of Co and Mo species calculated by using the Scherrer equation. The pore properties of the activated carbons and catalyst samples were estimated by nitrogen adsorption-desorption isotherm at 77 K using surface area analyzer (SAA, Quantachrome NovaWin Series). Prior to nitrogen adsorption-desorption studies, the samples were degassed at 300 °C for 3 h. The morphology of the sample was characterized by scanning electron microscopy (SEM, Jeoul JSM-6510). The samples were prepared by attaching carbonized Merbau woods to carbon tape, with a sputter-coated platinum layer on the sample surface at 15 kV accelerating voltage. TEM images were determined by the JEOL-JEM-1400 microscope at 120 kV.

3. Results and discussion

3.1. Characterization of MC

3.1.1. Crystallographic characterization

Structural changes were observed in the carbonized product as effect temperature carbonization under different hold times of carbonization. XRD patterns (Fig. 1a–d) show that the raw Merbau woods exhibits three peaks similar to those reported [30], the materials were from coconut shells of Malaysian variety. The results were in agreement with that of XRD patterns of microcrystalline cellulose [31] together with amorphous regions. All of the carbonized Merbau woods patterns exhibited two broad peaks, which typically represent amorphous carbon and have slightly crystalline structures [32]. The broad peaks centered at 2θ = 23° and 43° refer to (0 0 2) crystal plane of graphitic layer and (1 0 0) reflective planes in the structure of turbostratic carbon, suggesting randomly oriented graphitic layers in the material [33,34]. These findings are consistent with the carbonized from other reported [35–37].

Reflection located at 2θ ≈ 26°, related to the 002 graphite structure, is indicative of the stacking of a few graphene-like layers into the activated carbon, as a similar reviewed by González-García, characteristic for activated carbon from lignocellulosic precursors [38]. Fig. 1a–d showed the pattern assigned to the reflection from graphite. The results were in agreement with that of peaks commonly observed on biocarbon obtained from the temperature of carbonization 700–900 °C [39], for this reported stable peaks were obtained at 600–800 °C. This peak appears at all of the temperatures of carbonization 500–800 °C, however, were not observed at 3 h hold time of carbonization at 500 °C (MC53). It can be explained the characteristic feature of amorphous materials, indicating the pyrolysis converted the crystalline cellulose structure to an amorphous, random, disordered structure. The interlayer distance of the carbon layer of MC53 is higher than that for graphite 2θ = 26,55°), as shown in Table 1. This naturally found for porous biocarbon and can be due to the presence on the carbon surface of a large number of functional groups [37]. The interlayer spacing, $d_{0\,0}$

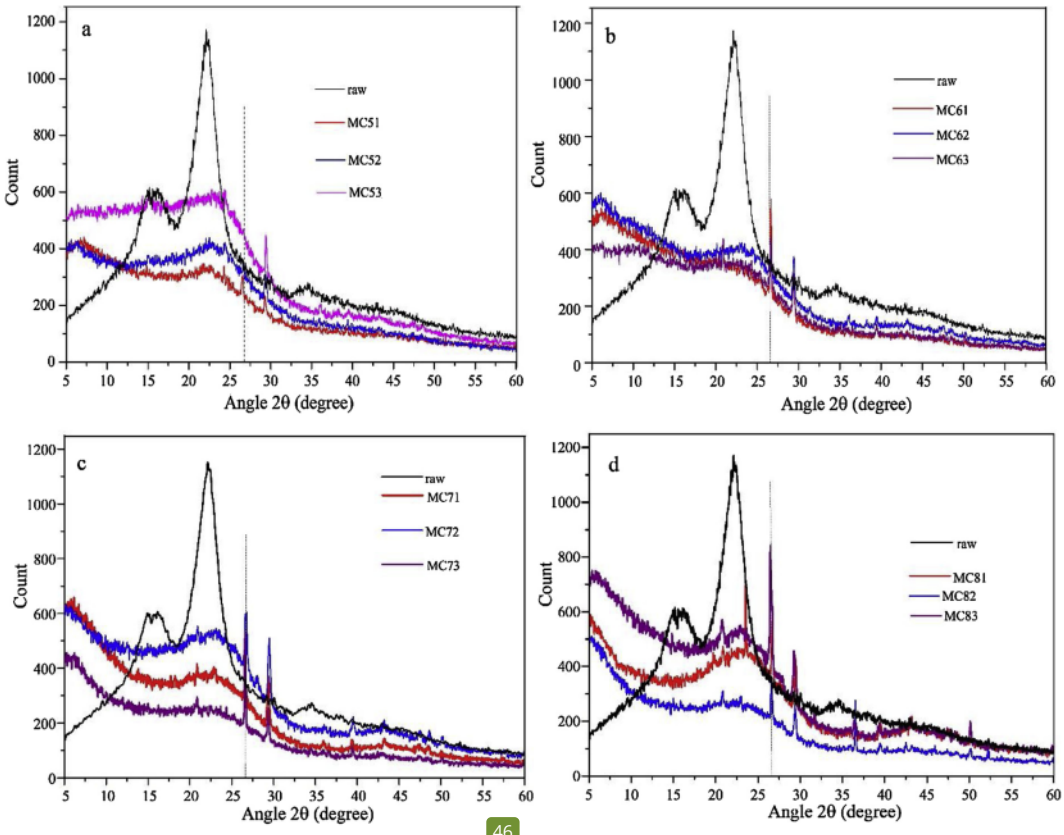

Fig. 1. XRD patterns of Merbau woods and the carbonized Merbau wood at different of temperatures: (a) 500, (b) 600, (c) 700, and (d) 800 °C temperature of carbonization.

Table 1
Interlayer spacing of 0 0 2 peaks of the carbonized sample.

Sample	2 θ	$d_{0\,0\,2}$	Sample	2 θ	$d_{0\,0\,2}$
	(°)	(nm)		(°)	(nm)
MC51	26.62	0.3345	MC71	26.6	0.3340
MC52	26.92	0.3308	MC72	26.69	0.3336
MC53	24.21	0.3672	MC73	26.59	0.3348
MC61	26.64	0.3342	MC81	26.67	0.3339
MC62	26.59	0.3348	MC82	26.57	0.3350
MC63	26.66	0.3340	MC83	26.46	0.3365
JCPDS No.010898487	26.55	0.3354			

$_2$, was calculated using the Bragg equation:

$$d = \frac{\lambda}{2sin\theta} \quad (2)$$

where λ is the wavelength and θ is the scaterring angle of the peak position.

When the temperature of carbonization increases from 600 to 800 °C the peak located at 2θ ≈ 26° observed has stabilized; other than that, the intensity and the sharpness of the peaks at these broad peaks increases. It shows an increase in the ordering of graphitic carbon layers at high temperatures [37]. The interlayer spacing in this range of temperature of carbonization is lower than graphite. It can be attributed to the effect of dehydration on the carbon structure due to the effect of heat, leading to a reduction of functional groups in the samples related to the spacing between the graphic layers of the interlayer. This type of interlayer spacing of carbon with intensely graphitic layers would influence the available surface area, as shown in Table 2.

3.1.2. Infrared analysis

FTIR spectra obtained with different temperatures were presented in Fig. 2a-d. The broadband at 3410 and 3425 cm^{-1} correspondings to the O−H stretching vibration mode of hydroxyl functional groups of alcohols, acids, and phenols. A weak peak at 2924 and 2854 cm^{-1} was associated with aliphatic and aromatic asymmetric C−H and symmetric C−H stretching bands. The existence of functional oxygenated groups was shown in the bands between 1000 − 1750 cm^{-1}. For example, the band at 1033 for Merbau woods spectra can be assigned to C−O), and δ (O−H), the band at 1705 for 600 and 700 °C, (Fig. 4b–c) was ascribed to C=O vibrations in carbonyl groups. The existence of the band in 1435 cm^{-1} at the temperature of carbonization of 600 and 700 °C indicates the presence of aromatic C, indicative of lignin C=C [40]. Aromatic C=C stretching present in olefinic vibrations in the aromatic region [41] shown at bands 1600 − 1500 cm^{-1}. Aromatic C−H bending can be found at 879, 871, and 871 cm^{-1} [40], for 800, 700, and 600 °C, respectively, and not observed at 500 °C. It was indicated that aromatic cluster can already be formed at these temperatures of pyrolysis. Furthermore, the analysis of functionalized groups with the existence of aromatic groups that was found at 600–800 °C temperature of carbonization was corresponding to carbon with highly graphitic layers characterization in Fig. 1b–d. The influence of temperatures on the yield of carbonized Merbau wood shown in supplementary information as Figure S2. It was shown that the yield of carbonized Merbau woods decreased rapidly when temperatures were below 600 °C, and gradually decreased at a temperature above 600 °C.

Carbonized from biomaterials is mainly consists of amorphous carbon with a highly functionalized surface, making it reactive to various compounds, such as inorganic and organic species [74]. These functionalized surfaces can be found as a large amount of oxygen-containing groups (i.e., carboxylic, lactonic, and phenolic). The surface functional group on carbon contributes significantly to the adsorption ability [43]. Boehm titration was possible to obtain an estimate of total acids groups, equivalent per gram of carbonized sample (meq/g) present in the sample surface, shown in Fig. 3. The carbonized samples showed a variation of total acid functional groups of 2.76–5.18 meq/g. In comparison, the total acid groups carbonized castor meal biomass sample of 4.77–7.98 meq/g [44]. Almost all of the variation on these pyrolysis condition reaction show phenolic as a contributor as acidic groups to obtain the total acidity on the samples carbonized Merbau woods, except for the condition of reaction at 800 °C under 2 h hold time of carbonization. Acidic groups of lactonic were not identified for all of the samples.

3.1.3. Morphology analysis

To further confirm the morphological features and pore shapes of carbonized Merbau woods, SEM analysis for selected carbonized samples (MC72 and MC83) was carried out and presented in Fig. 4. The SEM micrographs with magnification 1000x are shown in Fig. 4a–b. All of that selected carbon show few pores on these surfaces. However, a large number of different sizes and a honeycomb-shaped tunnel. The pore formed with cross-connected orientation and overlapped each other.

3.1.4. Pore structures analysis

The pore size distribution and average pore diameter were established by analyzing the N_2 adsorption data with The Barrett-Joyner-Halenda (BJH) method [45]. The characteristics of porosity in carbonized Merbau woods at various hold times of carbonization and

Table 2
Characteristics of porosity and acidity of carbonized Merbau woods, Co/MC72, and Mo/MC72.

Sample	S_{BET}[b] (m^2/g)	V_{total}[b] (cm^3/g)	V_{micro}[b] (cm^3/g)	V_{meso}[b] (cm^3/g)	$D_{average}$[b] (nm)	Acidity[a] (mmol/g)	Metals average size[c] (nm)
MC51	39.26	0.04	0.015	0.023	3.866	–	–
MC52	5.55	0.02	0.002	0.013	10.055	–	–
MC53	15.74	0.02	0.005	0.016	5.248	–	–
MC61	80.96	0.07	0.037	0.035	3.563	–	–
MC62	4.61	0.01	0.002	0.012	11.722	–	–
MC63	16.57	0.03	0.006	0.026	78.14	–	–
MC71	68.44	0.12	0.032	0.087	6.931	–	–
MC72	330.31	0.23	0.147	0.081	2.758	2.96	–
MC73	89.44	0.08	0.042	0.033	3.360	–	–
MC81	3.17	0.01	0.001	0.013	17.911	–	–
MC82	20.12	0.05	0.009	0.043	10.312	–	–
MC83	350.56	0.18	0.156	0.026	2.075	–	–
Co/MC72	384.7	0.197	0.147	0.005	2.015	3.62	2.64
Mo/MC72	53.57	0.039	0.005	0.034	5.337	3.86	6.10

[a] The acidity of the catalyst was determined gravimetrically using adsorption NH_3 basic of gas.
[b] S_{BET}, total volume, micropore volume, and diameter of the samples were calculated using BET, DR, and BJH theory, respectively.
[c] Particle size was calculated using the Scherrer equation.

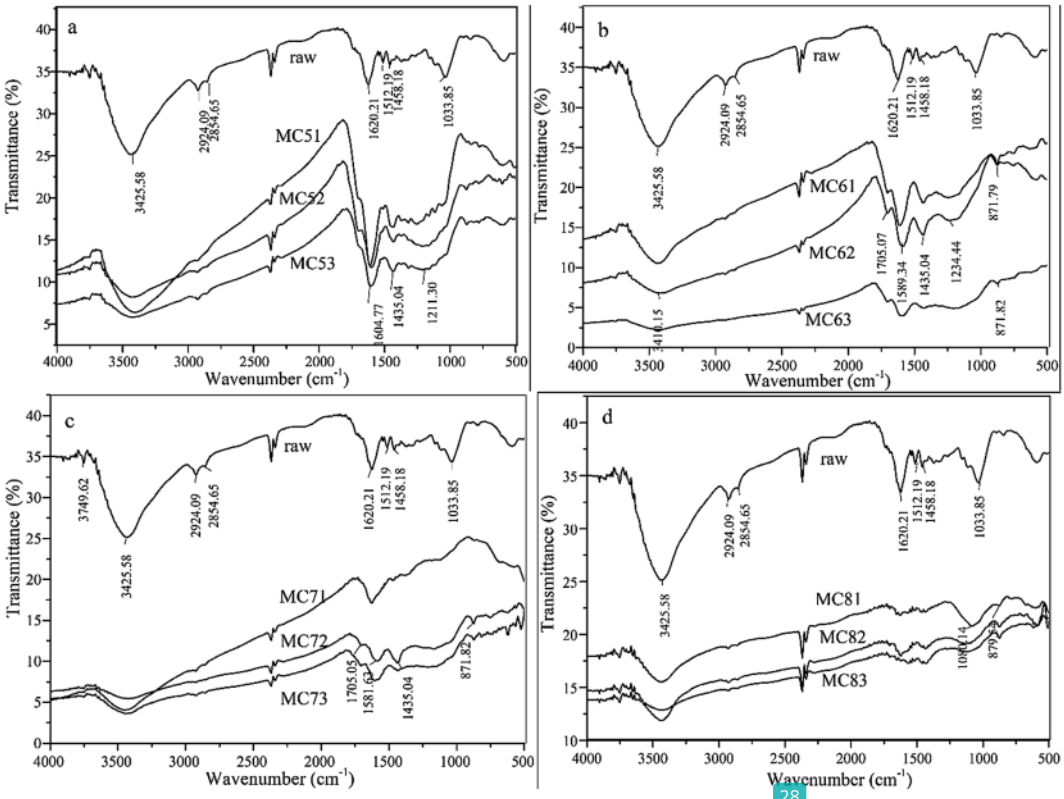

Fig. 2. FT-IR spectra of Merbau woods and carbonized Merbau wood hold time of 1, 2, and 3 h, and at (a) 500, (b) 600, (c) 700 and (d) 800 °C.

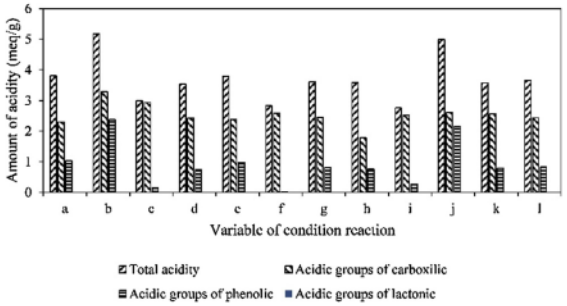

Fig. 3. Acidity based on total, acidic groups of carboxylic, phenolic, and lactonic (meq/g): (a) MC51, (b) MC52, (c) MC53, (d) MC61, (e) MC62, (f) MC63, (g) MC71, (h) MC72, (i) MC73, (j) MC81, (k) MC82 and (l) MC83.

temperature carbonization were shown in Fig. 5a–c and listed in Table 2. The developed mesostructured was observed in all the hold time and different temperature carbonized of carbonized Merbau woods. It can be seen that these mesoporous carbonized Merbau woods at hold time of carbonization 1 h posses a uniform pore size distribution at about 4 nm of 700 °C (shown in Fig. 5a), and at 2 h the carbonized samples showed a different range of uniform pore size, about 3.5 nm of the MC82 samples, as shown in Fig. 5b. In comparison, mesoporous with several different sizes of distributions also were observed on samples at 3 h of 600 °C (MC63), shown in Fig. 7c. The corresponding average diameter was summarized in Table 2, which showed that the MC63 was macroporous materials. This interpretation for MC63, however, related to the trend of curves of pore distribution (shown in Fig. 5c) and the type IV of N_2 adsorption-desorption isotherm (shown in Fig. 6b). MC63 has various pore size distribution, which is a mixture of mesoporous-macroporous materials.

N_2 adsorption-desorption isotherm of the four kinds of carbonized under the several holds of time is presented in Fig. 6. It reveals that the adsorption isotherms of the carbonized at 2 h of all temperatures (MC52, MC62, MC72, and MC82) are of type IV, as well at 1 h (700 °C, called as MC71), and at 3 h (600 °C, called as MC63), which is characteristic for mesoporous materials. These isotherm curves present the hysteresis loops type 4 (H4). Type H4 loops are sometimes correlated with narrow slit pores, includes activated carbon pores in the micropore region [46].

The adsorption isotherm at 1 h of 500 °C (MC51), 600 °C (MC61), and 800 °C (MC81) is of type II, as same at 3 h of 500 °C (MC53) and 700 °C (MC73) which is representative of non-porous and macroporous materials. In accordance with the classification adopted by the International Union of Pure and Applied Chemistry (IUPAC), micropore (diameter < 2 nm), mesopore (2 − 50 nm), and macropore (> 50 nm). The average pore diameter of MC51, MC61, MC81, MC53, and MC73 were in the range of 3 − 17 nm, which the pore sizes become predominantly non-porous and macroporous-mesoporous.

Correspondingly, Fig. 6d gives the N_2 adsorption-desorption isotherms of MC83. According to IUPAC classification, the MC83 profile was of type I and type II composite, suggesting a high volume of micropore and a significant amount of mesopore. Curve isotherm of MC83 shows that the high microporosity ($P/P_0 < 0.1$) is associated with the microporous filling, along with substantial mesoporosity in the range of $0.1 < P/P_0 < 0.99$. The BJH adsorption average pore diameter was 3.36 nm, which the samples pore sizes become microporous-mesoporous predominantly materials.

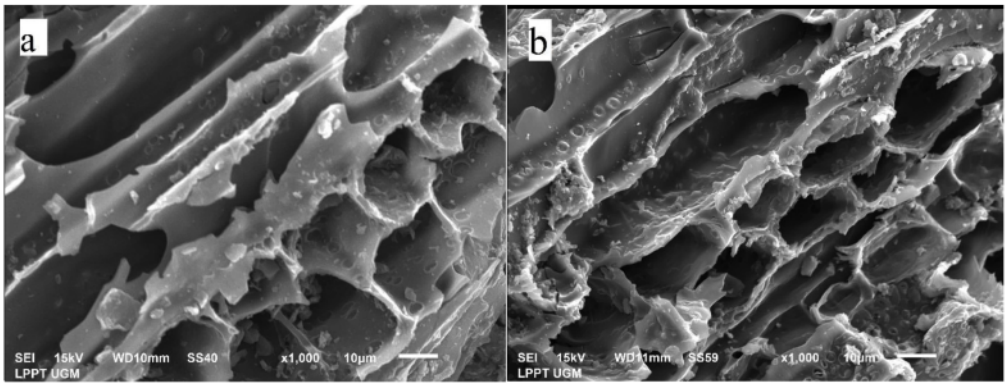

Fig. 4. SEM micrographs of selected carbonized Merbau woods at magnification 1000x: (a) MC72, and (b) MC83.

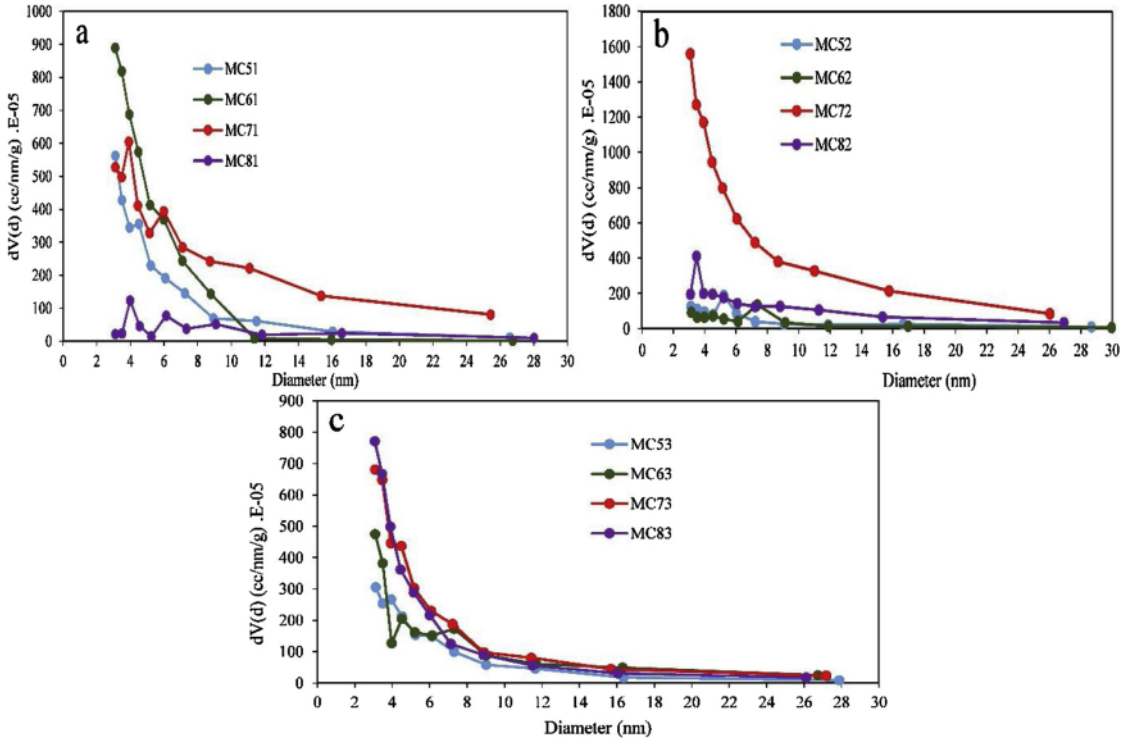

Fig. 5. Effect of the carbonization temperature of 500, 600, 700 and 800 °C on pore size distribution prepared at (a) 1, (b) 2, and (c) 2 h hold time of carbonization.

These carbonized samples generally show mesoporous structures. The BET surface area was calculated from the isotherms by using the Brunauer-Emmett-Teller (BET) equation [47]. The DR method was used to calculate the micropore volume [48]. Refer to the pyrolysis Merbau woods, these results confirm with the concept that hemicellulose, cellulose, and lignin will produce dehydration, linkage breaking off reactions, residual carbon structural ordering process, and finally occur polymerization reaction during the carbonization process [49]. As shown in Table 2, the BET surface area and micropore volume of the carbonized Merbau woods have the same trend at all different temperatures and hold time of carbonization. It was indicated that the increasing volume of micropore giving rise to increases in the BET surface area. The reports were consistent with the published ones [49].

BET surface area at 500 and 600 °C showed the same pattern as function as different hold time of carbonization, this phenomenon not only may be caused by linkage breaking off reactions that still occur at this temperatures but also indicating that carbonization and oxidation process created new pores during the activation and more previously inaccessible pore were opened. For example, the BET surface area of the carbonized samples at 2 h hold time of carbonization has decreased and got up at 3 h hold time of carbonization. This case has reversed at 700 °C temperature carbonization, of the MC72 and MC73 samples, which indicated the structural ordering process of the residual carbon. Although, the decreasing BET surface area at 3 h hold time of carbonization, which represents polymerization reaction during the carbonization process still not finished. The polymerization proses seen already started stable at 800 °C temperature of carbonization. It confirmed as increasing the BET surface area followed by developing

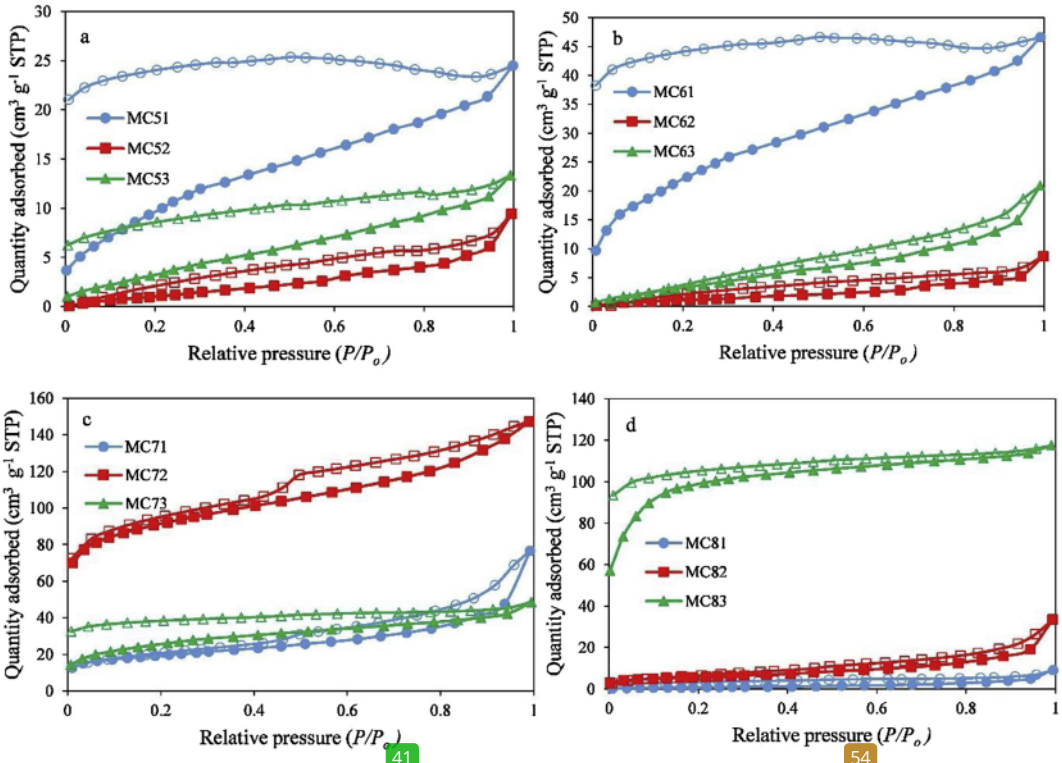

Fig. 6. Adsorption isotherm of the samples prepares at various temperature: (a) 500 °C, (b) 600 °C, (c) 700 °C, and (d) 800 °C. Filled and empty symbols represent the adsorption and desorption branches, respectively.

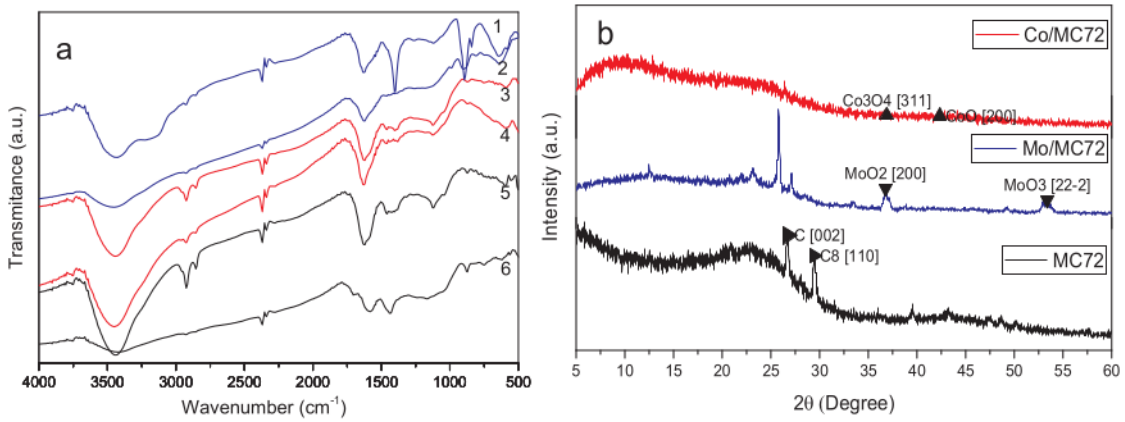

Fig. 7. (a) FT-IR spectra of (1) Mo/MC72-NH_3 absorbed, (2) Mo/MC72 before absorbed, (3) Co/MC72-NH_3 absorbed, (4) Co/MC72 before absorbed, (5) MC72-NH_3 absorbed, and (6)MC72 before absorbed; (b) XRD spectra on MC72, Co/MC72, and Mo/MC72 catalyst.

the volume total, and the volume of micropore as well as reducing the diameter of the pore. It also confirmed by XRD pattern, as shown in Fig. 1c–d and as demonstrated [35], the carbonized samples develop a more ordered structure in gasification with a slower rate at high carbonization temperatures.

3.2. Characterization of Co/MC72 and Mo/MC72 catalysts

XRD patterns of the MC72, Co/MC72, and Mo/MC72 catalyst shown in Fig. 7b. The impregnation of cobalt and molybdenum into the structure of MC showed that structural was not changed and typically of amorphous, random and disordered structure. The impregnation of cobalt results in peaks that correspond to the presence of Co_3O_4 and CoO in the Co/MC72 catalyst. Co_3O_4 corresponds to cubic structure (JCPDS: 42–1467) as characteristic diffraction peaks appeared 2θ of 36.8° [311]. The CoO cubic structure appeared at 42.38° [200] (JCPDS: 42–1300), also confirmed by EDX results (shown in supplementary information as Table S1). Molybdenum was present as MoO_2 [200] (JCPDS: 32-0671) at 36.76° and MoO_3 [22,2] (JCPDS: 47–1081) at 53.37° that corresponds to the monoclinic structure (confirmed by EDX

Table 3
The major product of pyrolyzed α-cellulose[a] via pyrolysis based on GC–MS data.

Compound	Mol.formula	Content (wt.%)
Anhydrosugars		22.32
1.4:3.6-dianhydro-α-D-glucopyranose	$C_6H_8O_4$	1.81
1.6-anhydro-β-D-glucopyranose(levoglucosan)	$C_6H_{10}O_5$	20.51
Aldehydes		1.51
2-Furancarboxaldehyde	$C_5H_4O_2$	0.86
2-Butenal	C_4H_6O	0.65
Ketones		17.28
1-Hydroxy-2-propanone	$C_3H_6O_2$	13.45
2.3-Pentanedione	$C_5H_8O_2$	0.12
2-Butanone	$C_4H_8O_2$	2.93
1-Hydroxy-2-butanone	$C_4H_8O_2$	0.35
1-Acetyloxy-2-propanone	$C_5H_8O_3$	0.43
Acids		10.18
Acetic acid	$C_2H_4O_2$	8.15
Propanone acid	$C_3H_6O_2$	2.03
Alcohols		–
Furans		1.17
2.5-Dimethylfuran	$C_6H_8O_4$	1.17
Phenols		–
Hydrocarbons		5.59
2.4-Dimethylpentane	C_7H_{16}	2.05
Pentane	C_5H_{12}	3.54
Others		11.37
Carbon dioxide	CO_2	7.27
1-Methylcyclopropanemethanol	$C_5H_{10}O$	0.56

[a] The yield of pyrolyzed α-cellulose (liquid fraction) is 71.98 wt.%.

results in supplementary information as Table S2).

The impregnation of cobalt and molybdenum into MC72 affected the acidity. The acidity of the support increasing due to the presence of metals, as presented in Table 3. The orbitals to accept an electron from the NH_3 molecule as basic adsorbate was provided by the oxide form of cobalt (CoO and Co_3O_4) and molybdenum (MoO and MoO_3), as a result of XRD spectra, shown in Fig. 7b. Consequently, metal has an act as Lewis acid (electron acceptor) [15]. Meanwhile, the acidity of the catalyst was also contributed by proton donator (Brönsted acid sites), which derived from the acidic functional group on the surface of material support (i.e., carboxylic and phenolic). One way to distinguish between Brönsted and Lewis acid sites was possible made by infrared spectroscopic studies of ammonia adsorbed [50,51].

The FTIR spectra of the MC72, Co/MC72 and Mo/MC72 catalyst after NH_3 gas sorption in acidity test were presented in Fig. 7a. The band at 1404 cm^{-1} (Co/MC72 and Mo/MC72) and 1427 cm^{-1} (MC72), were recognized as Brönsted acid sites, which is the characteristic peak of an ammonium ion and N−H bending vibration region [27,52]. The absorption peak at 1620 cm^{-1} MC72 and Co/MC72 samples and 1627 cm^{-1} of Mo/MC72, was contributed by ammonia coordinately bonded to the Lewis acid site [50]. The band at 1311.59 cm^{-1} was assigned to δ_s(H-*N*-H), which coordination to Co^{3+}, as reported by Xie et al. [52].

Fig. 8a and c showed the adsorption-desorption isotherm of the Co/MC72 and Mo/MC72 catalyst indicated that was of type II according to IUPAC classification, characteristic for nonporous and macroporous materials. The knee of the isotherm at (P/P_0 < 0.1) of Co/MC72 was sharper than the isotherm of MC72 (shown in Fig. 6c), indicated the presence of small fraction of micropore, which developed in the Co/MC72 samples due to formation of new micropores as an effect of the impregnation process. The Co/MC72 exhibited pores diameter 2.015 nm (shown in Table 2) which smaller than pore diameter of MC72 likely because partially blockage of mesoporous channels by cobalt and formation the new pore, as well as increased surface area and reduced the total pore volume and pore diameter of Co/MC7 materials. Furthermore, the particle size of the Co metal species allows for entry into meso-sized pores as in the data shown in Table 2, which is consistent with the above assumption and confirmed with the image of TEM (shown in Fig. 9d). In accordance with the porous classification adopted by IUPAC the average pore diameter of Co/MC72 was 2.015 nm, and most of the mesoporous is in the pore size range of 4 − 24 nm (shown in Fig. 8b), which the pore size becomes predominantly mesoporous, and macroporous-nonporous materials.

Mo particle size of the Mo/MC72 samples, which is larger than the pore diameter of the support causes the metal to be distributed on the outside even to close the meso-sized pore resulted in a sharp decrease in the surface area of the material and the total pore volume (Table 2). These metal particles may even be able to occupy macro-sized pores and causes the average diameter of the material to be larger than before the impregnation of the metal.

Figs. 9a and c showed the SEM images of the Co/MC72 and Mo/MC72 catalyst. These images show that the honeycomb-shaped tunnel on the catalyst. The surface morphology of all samples has similar to Activated Mesoporous Biocarbons (AMB) synthesized by Singh et al. originating from Arundo donax [37], but the samples produced from this research further uniform. The pore formed with cross-connected orientation and overlapped each other, as shown in the TEM figure of MC72 as support in Fig. 9e.

The details structure of the mesoporous MC72 and Co/MC72 catalyst can be provided by TEM analysis, shown in Fig. 9e–g. Fig. 9e exhibits the TEM images of the representative sample MC72 exhibited spherical morphology. These images have similar to those reported by Pillai and coworkers, which the use of carbon commercials [53]. This image reveals that there are several regular mesoporous channels in large domains, which are attached and connected, besides the amorphous carbons were observed. It should be mentioned that this image showed the structure before the cobalt enters the precursor system. Meanwhile, the uniform dark spots that are assigned to the cobalt nanoparticles, that can be detected in Fig. 9f. It is corresponding to the bright field and some parts in the form of layers, indicating that cobalt nanoparticles are dispersed into the walls of graphitic mesoporous carbon. This image confirm that decreasing total pore volume and average diameter may be caused by partial blockage of mesoporous channels by cobalt, which is consistent with the Scherrer evaluation of the average size of cobalt particles based on X-ray diffraction data. The further study of structure Co/MC72 as the catalyst of hydrocracking shown in Fig. 9g. This image reveals that after hydrocracking of pyrolyzed α-cellulose, the dark spot, which is cobalt nanoparticles, is quite darker, indicating that the formation of coke may cause catalyst deactivation.

3.3. Catalytic activity test of Co/MC72 and Mo/MC72 in hydrocracking of pyrolyzed α-cellulose

Bio-oil of α-cellulose has obtained by the pyrolysis process; after that, the hydrocracking can be done to investigation catalytic activity of the Co/MC72 sample. Pyrolysis was carried out in a stainless steel semi-batch reactor, shown in supplementary information as Figure S1. The pyrolysis products are a fraction of vapor consisting of H_2O and a complex mixture of organic compounds, carbon-rich solid, and an incondensable gas fraction (Table 3).

The prominent peaks in the spectra of pyrolyzed α-cellulose correspond to carbon dioxide as a volatile fraction that was into a liquid fraction, as were an agreement with the previous investigation by French and Czernik [9]. The top spectrum derived from cellulose pyrolysis reveals standard products of carbohydrate breakdown products such as acetic acid and levoglucosan. Levoglucosan (anhydrosugars of 22.32 wt.%) is the primary product of depolymerizing cellulose [9], in addition to furans (1.17 wt.%) [17]. The other compounds contained ketones (17.28 wt.%) which was formed by pyrolytic ring scission of holocellulose (cellulose and hemicellulose) [17]. Pyrolysis of α-cellulose gave some acids (10.18 wt.%), especially acetic acid which mainly derived from the deacetylation process. Due to their corrosivity and

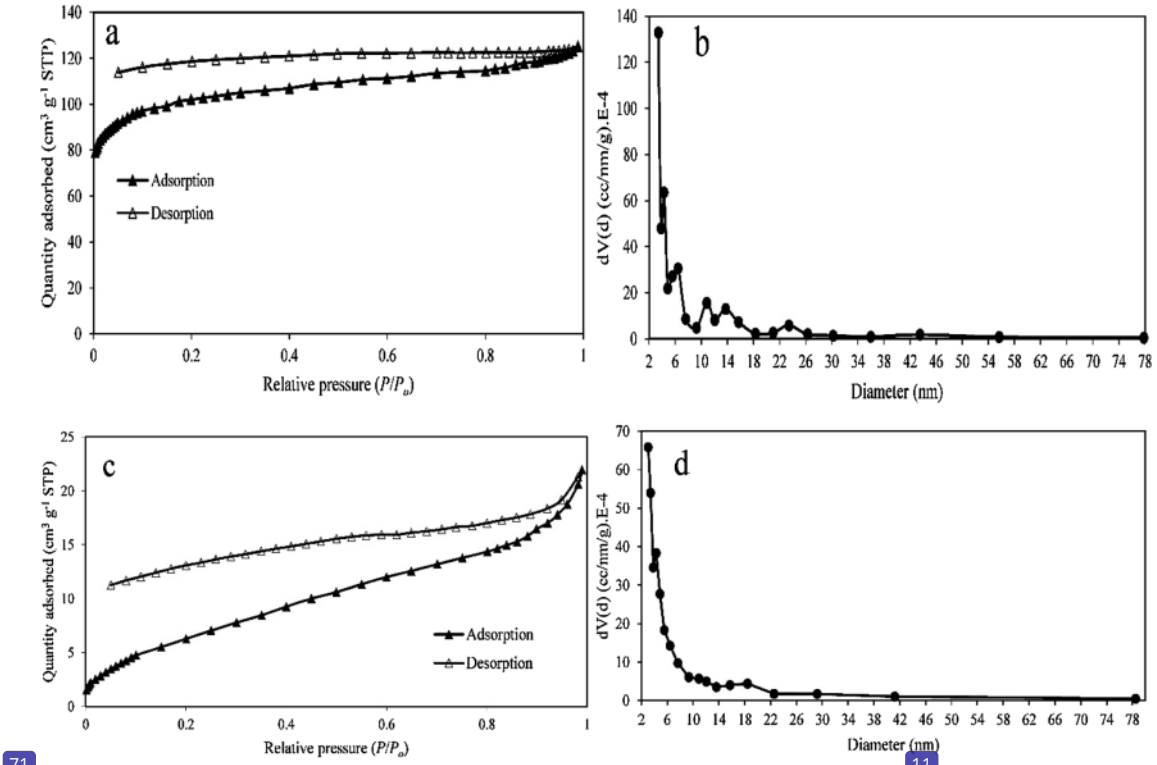

Fig. 8. N_2 adsorption-desorption isotherm of: (a) Co/MC72 and (c) Mo/MC72 catalyst. The pore size distribution of : (b) Co/MC72 and (d) Mo/MC72 catalyst.

influences on the ageing of bio-oils, the presence of acids will have negative effects on the properties of bio-oils. Other products from α-cellulose pyrolysis are aldehydes (1.51 wt.%), furans (1.17 wt%), hydrocarbons (5.59 wt.%), CO_2 gas (11.37 wt.%), and 1-methylcyclopropanemethanol (0.56 wt.%).

The upgrading of a liquid fraction as the product pyrolyzed α-cellulose performed with hydrocracking using the Co/MC72 and Mo/MC72 catalyst. This process has included hydrodeoxygenation because as well as deoxygenation reactions, hydrogenation, can occur [15]. Table 4 showed the product distribution and the selectivity of the liquid product of the hydrocracking process. The results showed that the product has three phases were a gas fraction, coke, and liquid fraction. Thermal hydrocracking produced the lowest liquid product than the catalytic hydrocracking by using Co/MC72 and Mo/MC72. This could happen due to the formation of radical ions triggered by high temperatures. The longer carbon chains were produced by the formation of carbocations in the catalytic hydrocracking. This leads to an increase in liquid products.

In general, thermal and catalytic hydrocracking exhibited cracking capabilities, it is indicated by completely eliminated anhydrosugar compounds as a major product of the pyrolysis process. Cellulose's pyrolytic ring break formed different light products, mostly linear carbonyls [17]. Throughout transport and storage, ketones and aldehydes are undesirable products that are attributed to the instability of bio-oil [19]. 2-furancarboxaldehyde and 1-hydroxy-2-propanone were the most abundant aldehydes and ketones in the pyrolytic products, respectively. After catalysis, the 2-furancarboxaldehyde was increased, while the 1-hydroxy-2-propanone was reduced by thermal and Co/MC72. Whereas, these compounds eliminated by Mo/MC72. The total of linear carbonyls was reduced by thermal (14.89 wt.%) and Co/MC72 (16.13 wt.%), while the pyrolytic product percentage higher than these products (17.93 wt.%). Meanwhile, the main ketones as light linear carbonyls (acetone of 42.48 wt.%) were produced selectively by Mo/MC72. The thermal and Co/MC72 significantly increased the cyclic carbonyls (2-furancarboxaldehyde, 5-metil-2-furaldehyde, 2-metil-2-siklopenten-1-one, 3-metil-2-siklopenten-1-one, 3-metil-1,2-siklopentanadion).

According to Table 4, the acids that were produced by the pyrolytic process (10.18 wt%) were slightly reduced by Mo/MC72 (7.30 wt.%) but increased by the thermal (16.49 wt%) and Co/MC72 (24.81 wt%). Previous studies have confirmed that catalytic cracking by most catalysts may promote acid formation [17,54]. Acids are responsible for bio-oil corrosiveness and therefore considered unwanted [19].

Alcohol compounds were produced by thermal, and Co/MC72. Alcohol is one of the desirable bio-oil upgrading ingredients for the production of biofuels, in addition to hydrocarbon compounds [19]. The highest total content is given by the thermal product (17.28 wt.%), and by Co/MC72 of 6.4 wt.%, while the Mo/MC72 does not give any alcohol products. Other than that, furan and phenol are also known to be substances high added value, therefore included in the desired product [19], and high yields of these compounds will help make the process more competitive economically [8]. Furan compounds were detected in the pyrolytic and Co/MC72 products, and they are known to be formed from dehydration of carbohydrates [55]. In general, thermal and catalytic hydrocracking exhibited cracking capabilities, Co/MC72 catalyst give increasing the product percentage (wt.%) of the light furans (2-hydroxytetrahydrofuran and 2-acetylfuran), while it decreased 2.5-dimethylfuran from the pyrolytic product. The thermal and Mo/MC72 product does not give the furans compounds. The other form of furans as the aldehydes compounds, the increasing of this type, gave from thermal and Co/MC72 products, but not by Mo/MC72 product.

The phenolic compounds are also a type of product in the pyrolyzed cellulose cracking reaction. Based on the cellulose pyrolysis reaction, there are no phenol compounds contained in bio-oil. The phenols

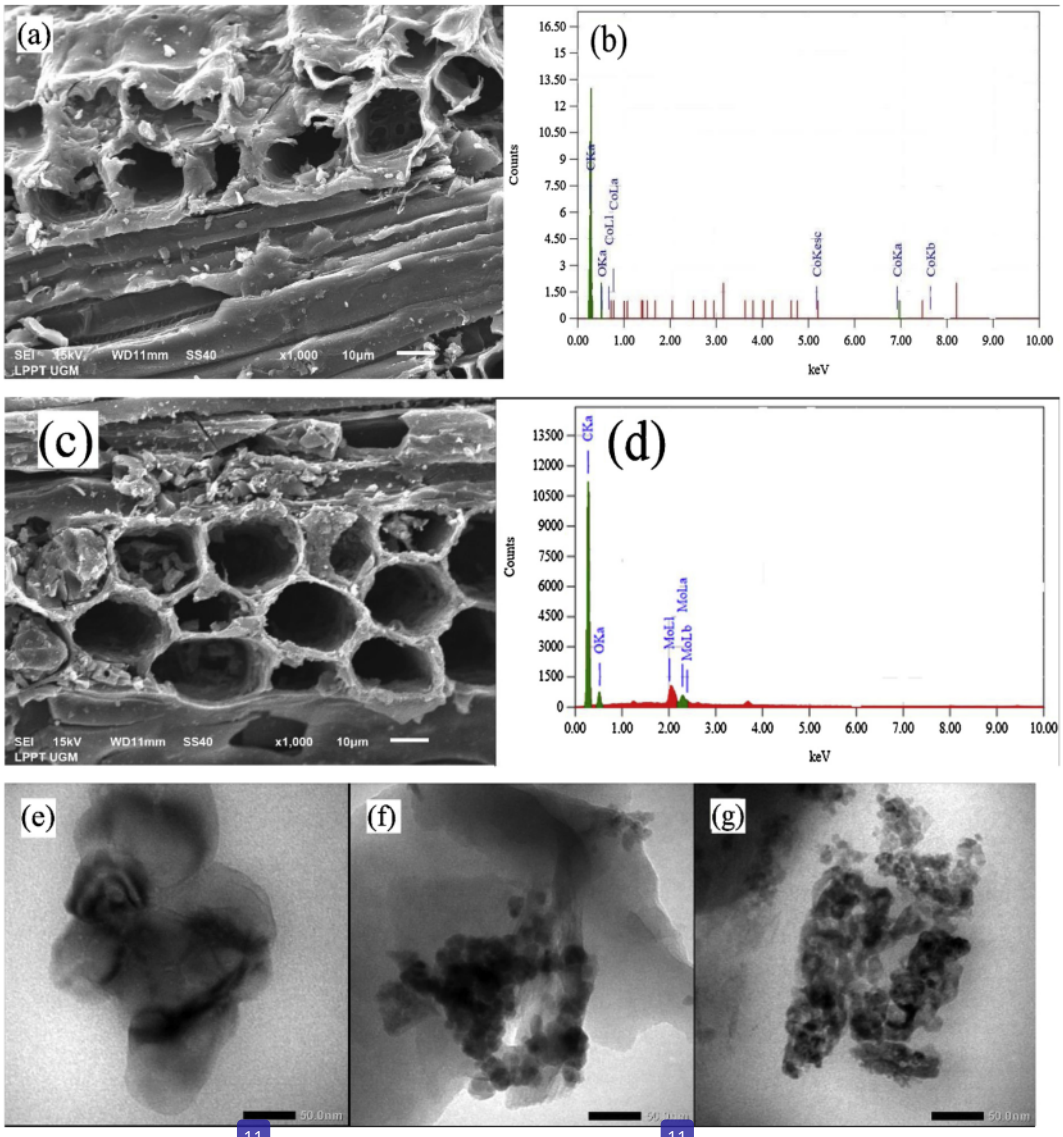

Fig. 9. Electron micrographs: SEM of: (a) Co/MC72 and (c) Mo/MC72 catalyst. EDX spectra of: (b) Co/MC72 and (d) Mo/MC72 catalyst. TEM image: (e) MC72, (f) Co/MC72 fresh catalyst, (g) Co/MC72 used catalyst.

produced in a catalytic hydrocracking reaction is likely to originate from a secondary reaction of other oxygenated compounds from bio-oil. In this work, the Co/MC72 catalyst showed selectivity for the phenols. How ever, it did not produce by thermal and Mo/MC72. According to the results, the Co/MC72 gives the light phenols (phenol and 2-metilphenol) of 2.25 wt.%.

The Co/MC72 and Mo/MC72 catalyst increased the hydrocarbons yield of 12.67 wt.% and 24.90 wt.%, respectively, compared with 2.05 wt.% before the catalytic process. The thermal hydrocracking did not give the hydrocarbons yield. Suchamalawong et al. described that decarboxylation produces releasing oxygen from thermal cracking, whereas the catalytic cracking can convert large hydrocarbons to smaller hydrocarbons via decarboxylation and decarbonylation reactions [6]. These results were indicating that these catalysts were effective in hydrodeoxygenation and hydrocracking bio-oil. Catalytic reactions occur through the formation of carbocations as intermediates. This reaction can involve protonation reactions by the Bronsted acid site or the H-abstraction of the Lewis acid site. The carbocations can undergo a number of reactions. By alkyl shift, they can isomerize into intermediates. Through β-scission, they will break into smaller molecules.

The percentage product of hydrocarbon compounds was 11.56 wt.% for propane and 1.11 wt.% for 4-Methyl-1-pentene by Co/MC72. Moreover, Mo/MC72 produced 2-Deutero-2-methylpropane (24.90 wt. %). 2-Deutero-2-methylpropane has a similar compound as 2-methylpropane. Based on the previous researches, the research octane number (RON) and motor octane number (MON) values for hydrocarbon fuels forming gasoline, respectively for propane were 111 and 96.6, while for 4-methyl-1-pentene was 98.9 and 85.1, and 2-methylpropane was 102.1 and 97.0 [56]. Accordingly, propane was the most preferable

Table 4
The product distribution and the selectivity of the liquid product of the hydrocracking process of pyrolyzed α-cellulose.

Catalyst	Hydrocracking product (wt.%)				
	Liquid fraction	Gas fraction	Coke	Residue	
Thermal	52.72	46.15	–	1.73	
Co/MC72	75.33	19.41	5.24	0.02	
Mo/MC72	74.69	25.18	0.13	0.01	
Compound		Mol.formula	Product percentage (wt.%)		
			Thermal[a]	Co/MC72[b]	Mo/MC72[c]
Anhydrosugars			–	–	–
Aldehydes			4.05	7.28	–
Butyraldehyde		C_4H_8O	–	0.51	–
2-Furancarboxaldehyde		$C_5H_4O_2$	4.05	4.94	–
5-Metil-2-furaldehyde		$C_6H_6O_2$	–	1.78	–
Ketones			14.89	18.29	42.48
Acetone		C_3H_6O	3.91	–	42.48
1-Hydroxy-2-propanone		$C_3H_6O_2$	7.22	9.81	–
3-Hydroxy-2-butanone		$C_4H_8O_2$	2.31	2.54	–
1-Hydroxy-2-butanone		$C_4H_8O_2$	–	1.20	–
2.3-Butanedione		$C_4H_6O_2$	1.45	–	
3-Penten-2-one		C_5H_8O	–	2.07	–
2-Metil-2-siklopenten-1-one		C_6H_8O	–	0.69	–
3-Metil-2-siklopenten-1-one		C_6H_8O	–	1.23	–
Metil-1,2-siklopentanadion		$C_6H_8O_2$	–	0.75	–
Acids			16.49	24.81	7.30
Formic acid		CH_2O_2	–	1.36	–
Acetic acid		$C_2H_4O_2$	13.42	17.05	7.30
Propanoic acid		$C_3H_6O_2$	3.07	4.80	–
Butanoic acid		$C_4H_8O_2$	–	1.60	–
Alcohols			17.28	6.4	–
2-Propenol		C_3H_6O	1.64	1.95	–
1-Propanol		C_3H_8O	–	2.78	–
Isobutil alkohol-2-D1		C_4H_9DO	15.64	–	–
2-Furanmethanol		$C_5H_6O_2$	–	1.67	–
Furans			–	1.54	–
2-Hidroxytetrahydrofuran		$C_4H_8O_2$	–	1.08	–
2-Acetylfuran		$C_6H_6O_2$	–	0.46	–
Phenols			–	2.25	–
Phenol		C_6H_6O	–	1.23	–
2-Metilphenol		C_7H_8O	–	1.02	–
Hydrocarbons			–	12.67	24.90
Propane		C_3H_8	–	11.56	–
2-Deutero-2-methylpropane		C_4H_9D	–	–	24.90
4-Methyl-1-pentene		C_6H_{12}	–	1.11	–
Others			–	2.49	–
Vinyl acetate		$C_4H_6O_2$	–	0.63	–
Butyrolactone		$C_4H_6O_2$	–	1.20	–
Acetol acetate		$C_5H_8O_3$	–	0.66	–

[a] The yield of hydrocracking of liquid phase pyrolyzed α-cellulose (liquid fraction) by thermal is 52.72 wt.%.
[b] The yield of hydrocracking of liquid phase pyrolyzed α-cellulose (liquid fraction) by Co/MC72 catalyst is 75.33 wt.%.
[c] The yield of hydrocracking of liquid phase pyrolyzed α-cellulose (liquid fraction) by Mo/MC72 catalyst is 74.69 wt.%.

than 4-methyl-1-pentene and 2-methylpropane because it has a higher octane number.

In addition, many other products were detected at a low level in the Co/MC72 products, such as vinyl acetate, butyrolactone, and acetol acetate. Ester compounds (vinyl acetate and acetol acetate) of 1.29 wt.%, and cyclic esters (butyrolactones) of 1.20 wt.%. Organic acids formed esters with water-removing alcohols [14].

Hydrodeoxygenation process, both through thermal and catalytic accomplished to decrease oxygenated compounds that contained on product liquid pyrolyzed α-cellulose, the desirable product of 6.76 wt.% (contained as furans and hydrocarbons) from the pyrolytic process increasing by the thermal of 17.28 wt.% (contained as alcohols), moreover by the Co/MC72 of 22.86 wt.% (consisted by alcohols, furans, phenols, and hydrocarbons) and catalytic by Mo/MC72 of 24.9 wt.% (selective product as hydrocarbons). The undesirable product from the pyrolytic process of 59.12 wt.% (contained as anhydrosugars, aldehydes, ketones, and acids) decreased into 35.43 wt.% by thermal hydrocracking, 52.87 wt.% by Co/MC72, and 49.78 wt.% by Mo/MC72 (consisted by ketones and acids). All of the hydrocracking processes could be observed with the absence of the levoglucosan, however, as the major product in pyrolyzed α-cellulose.

4. Conclusion

The product at higher temperatures and hold time of carbonization of Merbau woods increase volatile compounds, design more micropores, decrease in yield, and increase the total volume, microporous volume, and BET surface area. Furthermore, these would increase the aromatic groups and provide variations in the acidity of the carbonized Merbau woods. The characteristic feature of amorphous materials was shown the lowest carbonization temperature, indicating that pyrolysis converted the crystalline cellulose structures into an amorphous, random, disordered structure. At the higher temperature of carbonization, the carbonized Merbau woods acquire is indicative of the stacking of a few graphene-like layers into the activated carbon observed that have stabilized. Moreover, this ordered crystal would affect the available pore development. The optimal BET surface area, total volume and microporous volume of the carbonized Merbau woods prepared at 800

°C, 3 h hold time of carbonization (MC83) were 350.56 m^2/g, 0.18 cm^3/g, 0.186 cm^3/g. The pore size of the carbonized at this work shows the mesoporous, with a range of diameter were 2.075–11.722 nm.

The synthesized mesopore carbon as support cobalt and molybdenum metals, Co/MC72 and Mo/MC72, was tested catalytic selectivity on hydrocracking of pyrolyzed α-cellulose. This material catalyst was selected to hydrocarbon compounds of propane and 4-methyl-1-pentene (catalytic by Co/MC72) and selectively by Mo/MC72 to 2-deutero-2-methylpropane. The results of this work provide insight into designing carbonized materials with high surface area by carbonization temperatures and hold time carbonization followed by oxidation for adequate catalyst support. In addition, the metallic Co and Mo species can promote hydrodeoxygenation and deoxygenation (decarbonylation and decarboxylation) reactions that favor the production of hydrocarbons on the acid site of catalyst.

Author Contributions Statement

Darma Santi, Triyono, Wega Trisunaryanti, and Iip Izul Falah conceived and designed the experiments.

Darma Santi, Triyono, Wega Trisunaryanti, and Iip Izul Falah performed the experiments.

Darma Santi, Triyono, and Wega Trisunaryanti analyzed and interpreted the data.

Darma Santi, Triyono, Wega Trisunaryanti, and Iip Izul Falah contributed reagents, materials, reactors, analysis tools or data.

Darma Santi, Triyono, Wega Trisunaryanti, and Iip Izul Falah wrote the paper.

All authors provided critical feedback and helped shaped the research, analysis, and manuscript.

Declaration of Competing Interest

None.

Acknowledgements

This work was financially supported by the Ministry of research, technology, and higher education-BUDI DN and Ministry of Finance-LPDP- Republic of Indonesia (grant number: PRJ-4910/LPDP.3/2016).

References

[1] J. Grams, M. Niewiadomski, A.M. Ruppert, W. Kwapiński, Catalytic performance of a Ni catalyst supported on CeO2, ZrO2 and CeO2-ZrO2 in the upgrading of cellulose fast pyrolysis vapors, Comptes Rendus Chim. 18 (2015) 1223–1228, https://doi.org/10.1016/j.crci.2015.03.004.

[2] M. Rezaei, M. Mehrpooya, Investigation of a new integrated biofuel production process via fast pyrolysis, co-gasification and hydroupgrading, Energy Convers. Manage. 161 (2018) 35–52, https://doi.org/10.1016/j.enconman.2018.01.078.

[3] G. Zeng, L. Huang, Q. Huang, M. Liu, D. Xu, H. Huang, Z. Yang, F. Deng, X. Zhang, Y. Wei, Rapid synthesis of MoS 2 -PDA-Ag nanocomposites as heterogeneous catalysts and antimicrobial agents via microwave irradiation, Appl. Surf. Sci. 459 (2018) 588–595, https://doi.org/10.1016/j.apsusc.2018.07.144.

[4] I. Matos, E. Pérez-Mayoral, E. Soriano, A. Zukal, R.M. Martín-Aranda, A.J. López-Peinado, I. Fonseca, J. Čejka, Experimental and theoretical study of pyrazole N-alkylation catalyzed by basic modified molecular sieves, Chem. Eng. J. 161 (2010) 377–383, https://doi.org/10.1016/j.cej.2009.09.040.

[5] H. Serafim, I.M. Fonseca, A.M. Ramos, J. Vital, J.E. Castanheiro, Valorization of glycerol into fuel additives over zeolites as catalysts, Chem. Eng. J. 178 (2011) 291–296, https://doi.org/10.1016/j.cej.2011.10.004.

[6] P. Suchamalawong, S. Pengnarapat, P. Reubroycharoen, T. Vitidsant, Biofuel preparation from waste chicken fat using coal fly ash as a catalyst: Optimization and kinetics study in a batch reactor, J. Environ. Chem. Eng. 7 (2019) 103155, , https://doi.org/10.1016/j.jece.2019.103155.

[7] M. Li, F. Xu, H. Li, Y. Wang, Nitrogen-doped porous carbon materials: promising catalysts or catalyst supports for heterogeneous hydrogenation and oxidation, Catal. Sci. Technol. 6 (2016) 3670–3693, https://doi.org/10.1039/C6CY00544F.

[8] S.D. Stefanidis, K.G. Kalogiannis, E.F. Iliopoulou, A.A. Lappas, P.A. Pilavachi, In-situ upgrading of biomass pyrolysis vapors: catalyst screening on a fixed bed reactor, Bioresour. Technol. 102 (2011) 8261–8267, https://doi.org/10.1016/j.biortech.2011.06.032.

[9] R. French, S. Czernik, Catalytic pyrolysis of biomass for biofuels production, Fuel Process. Technol. 91 (2010) 25–32, https://doi.org/10.1016/j.fuproc.2009.08.011.

[10] A.R. Teixeira Cardoso, N.M. Conrado, M.C. Krause, T.R. Bjerk, L.C. Krause, E.B. Caramão, Chemical characterization of the bio-oil obtained by catalytic pyrolysis of sugarcane bagasse (industrial waste) from the species Erianthus arundinaceus, J. Environ. Chem. Eng. 7 (2019) 102970, , https://doi.org/10.1016/j.jece.2019.102970.

[11] T.S. Kim, S. Oh, J.Y. Kim, I.G. Choi, J.W. Choi, Study on the hydrodeoxygenative upgrading of crude bio-oil produced from woody biomass by fast pyrolysis, Energy. 68 (2014) 437–443, https://doi.org/10.1016/j.energy.2014.03.004.

[12] J. Adam, E. Antonakou, A. Lappas, M. Stocker, M.H. Nilsen, A. Bouzga, J.E. Hustad, G. Oye, In situ catalytic upgrading of biomass derived fast pyrolysis vapours in a fixed bed reactor using mesoporous materials, Microporous Mesoporous Mater. 96 (2006) 93–101, https://doi.org/10.1016/j.micromeso.2006.06.021.

[13] E.F. Iliopoulou, E.V. Antonakou, S.A. Karakoulia, I.A. Vasalos, A.A. Lappas, K.S. Triantafyllidis, Catalytic conversion of biomass pyrolysis products by mesoporous materials: effect of steam stability and acidity of Al-MCM-41 catalysts, Chem. Eng. J. 134 (2007) 51–57, https://doi.org/10.1016/j.cej.2007.03.066.

[14] J. Adam, M. Blazsó, E. Mészáros, M. Stöcker, M.H. Nilsen, A. Bouzga, J.E. Hustad, M. Grønli, G. Øye, Pyrolysis of biomass in the presence of Al-MCM-41 type catalysts, Fuel. 84 (2005) 1494–1502, https://doi.org/10.1016/j.fuel.2005.02.006.

[15] W. Trisunaryanti, E. Suarsih, I.I.F. Triyono, Well-dispersed nickel nanoparticles on the external and internal surfaces of SBA-15 for hydrocracking of pyrolyzed α-cellulose, RSC Adv. 9 (2019) 1230–1237, https://doi.org/10.1039/c8ra09034c.

[16] M. Stocker, Biofuels and biomass-to-Liquid fuels in the biorefinery: catalytic conversion of lignocellulosic biomass using porous materials, Angew. Chemie Int. Ed. 47 (2008) 9200–9211, https://doi.org/10.1002/anie.200801476.

[17] Q. Lu, Z.F. Zhang, C.Q. Dong, X.F. Zhu, Catalytic upgrading of biomass fast pyrolysis vapors with nano metal oxides: an analytical Py-GC/MS study, Energies 3 (2010) 1805–1820, https://doi.org/10.3390/en3111805.

[18] K. Murata, V. Sricharoenchaikul, Y. Liu, M. Inaba, I. Takahara, Effect of metal-modifed carbon catalysts on fast pyrolysis of Jatropha waste, J. Japan Pet. Inst. 56 (2013) 371–380, https://doi.org/10.1627/jpi.56.371.

[19] E.F. Iliopoulou, S.D. Stefanidis, K.G. Kalogiannis, A. Delimitis, A.A. Lappas, K.S. Triantafyllidis, Catalytic upgrading of biomass pyrolysis vapors using transition metal-modified ZSM-5 zeolite, Appl. Catal. B Environ. 127 (2012) 281–290, https://doi.org/10.1016/j.apcatb.2012.08.030.

[20] J. Han, H. Kim, The reduction and control technology of tar during biomass gasification/pyrolysis: an overview, Renew. Sustain. Energy Rev. 12 (2008) 397–416, https://doi.org/10.1016/j.rser.2006.07.015.

[21] W. Trisunaryanti, I.I. Falah, H. Susanto, Synthesis of mesoporous silica using gelatin as a template and Cr / silica catalyst for hydrocracking of waste lubricant oil, Int. J. Chemtech Res. 9 (2016) 388–397.

[22] M. Lu, X. Liu, Y. Li, Y. Nie, X. Lu, D. Deng, Q. Xie, J. Ji, Hydrocracking of bio-alkanes over Pt/Al-MCM-41 mesoporous molecular sieves for bio-jet fuel production, J. Renew. Sustain. Energy. 8 (2016) 053103, , https://doi.org/10.1063/1.4962561.

[23] W.M.A.W. Daud, W.S.W. Ali, M.Z. Sulaiman, The effects of carbonization temperature on pore development in palm-shell-based activated carbon, Carbon N. Y. 38 (2000) 1925–1932, https://doi.org/10.1016/S0008-6223(00)00028-2.

[24] J. Grams, M. Niewiadomski, A.M. Ruppert, W. Kwapiński, Influence of Ni catalyst support on the product distribution of cellulose fast pyrolysis vapors upgrading, J. Anal. Appl. Pyrolysis 113 (2015) 557–563, https://doi.org/10.1016/j.jaap.2015.03.011.

[25] M. Bartoli, L. Rosi, A. Giovannelli, P. Frediani, M. Frediani, Pyrolysis of α-cellulose using a multimode microwave oven, J. Anal. Appl. Pyrolysis 120 (2016) 284–296, https://doi.org/10.1016/j.jaap.2016.05.016.

[26] A.D. Prasiwi, W. Trisunaryanti, T. Triyono, I.I. Falah, D. Santi, M.F. Marsuki, Synthesis of mesoporous carbon from merbau wood (*Intsia spp.*) by microwave method as Ni catalyst support for α-Cellulose hydrocracking, Indones. J. Chem. 19 (2019) 575–582, https://doi.org/10.22146/ijc.34189.

[27] C.C. Huang, H.S. Li, C.H. Chen, Effect of surface acidic oxides of activated carbon on adsorption of ammonia, J. Hazard. Mater. 159 (2008) 523–527, https://doi.org/10.1016/j.jhazmat.2008.02.051.

[28] L. Li, P.A. Quinlivan, D.R.U. Knappe, Effects of activated carbon surface chemistry and pore structure on the adsorption of organic contaminants from aqueous solution, Carbon 40 (2002) 2085–2100, https://doi.org/10.1016/S0008-6223(02)00069-6.

[29] S.L. Goertzen, K.D. Thériault, A.M. Oickle, A.C. Tarasuk, H.A. Andreas, Standardization of the Boehm titration. Part I. CO2expulsion and endpoint determination, Carbon 48 (2010) 1252–1261, https://doi.org/10.1016/j.carbon.2009.11.050.

[30] A. Jain, S. Jayaraman, R. Balasubramanian, M.P. Srinivasan, Hydrothermal pretreatment for mesoporous carbon synthesis: enhancement of chemical activation, J. Mater. Chem. A Mater. Energy Sustain. 2 (2014) 520–528, https://doi.org/10.1039/C3TA12648J.

[31] M.L. Nieva, M.A. Volpe, E.L. Moyano, Catalytic and catalytic free process for cellulose conversion: fast pyrolysis and microwave induced pyrolysis studies, Cellulose 22 (2015) 215–228, https://doi.org/10.1007/s10570-014-0484-z.

[32] W. Kong, F. Zhao, H. Guan, Y. Zhao, H. Zhang, B. Zhang, Highly adsorptive mesoporous carbon from biomass using molten-salt route, J. Mater. Sci. 51 (2016) 6793–6800, https://doi.org/10.1007/s10853-016-9966-8.

[33] H. Shang, Y. Lu, F. Zhao, C. Chao, B. Zhang, H. Zhang, Preparing high surface area porous carbon from biomass by carbonization in a molten salt medium, RSC Adv. 5 (2015) 75728–75734, https://doi.org/10.1039/C5RA12406A.

[34] E. Altintig, S. Kirkil, Preparation and properties of Ag-coated activated carbon

nanocomposites produced from wild chestnut shell by ZnCl2 activation, J. Taiwan Inst. Chem. Eng. 63 (2016) 180–188, https://doi.org/10.1016/j.jtice.2016.02.032.
[35] Q. Yan, C. Wan, J. Liu, J. Gao, F. Yu, J. Zhang, Z. Cai, Iron nanoparticles in situ encapsulated in biochar-based carbon as an effective catalyst for the conversion of biomass-derived syngas to liquid hydrocarbons, Green Chem. 15 (2013) 1631, https://doi.org/10.1039/c3gc37107g.
[36] P.C. Bhomick, A. Supong, R. Karmaker, M. Baruah, C. Pongener, D. Sinha, Activated carbon synthesized from biomass material using single-step KOH activation for adsorption of fluoride: experimental and theoretical investigation, Korean J. Chem. Eng. 36 (2019) 551–562, https://doi.org/10.1007/s11814-019-0234-x.
[37] G. Singh, K.S. Lakhi, I.Y. Kim, S. Kim, P. Srivastava, R. Naidu, A. Vinu, Highly Efficient Method for the Synthesis of Activated Mesoporous Biocarbons with Extremely High Surface Area for High-Pressure CO2 Adsorption, ACS Appl. Mater. Interfaces 9 (2017) 29782–29793, https://doi.org/10.1021/acsami.7b08797.
[38] P. González-García, Activated carbon from lignocellulosics precursors: a review of the synthesis methods, characterization techniques and applications, Renewable Sustainable Energy Rev. 82 (2017) 1393–1414, https://doi.org/10.1016/j.rser.2017.04.117.
[39] C. Pham-Huu, C. Bouchy, T. Dintzer, G. Ehret, C. Estournes, M.J. Ledoux, High surface area silicon carbide doped with zirconium for use as catalyst support. Preparation, characterization and catalytic application, Appl. Catal. A Gen. 180 (1999) 385–397, https://doi.org/10.1016/S0926-860X(98)00371-8.
[40] K. Qian, A. Kumar, K. Patil, D. Bellmer, D. Wang, W. Yuan, R.L. Huhnke, Effects of biomass feedstocks and gasification conditions on the physiochemical properties of char, Energies. 6 (2013) 3972–3986, https://doi.org/10.3390/en6083972.
[41] M.L. Nieva Lobos, J.M. sieben, V. Comignani, M. Duarte, M.A. Volpe, E.L. Moyano, Biochar from pyrolysis of cellulose: an alternative catalyst support for the electro-oxidation of methanol, Int. J. Hydrogen Energy 41 (2016) 10695–10706, https://doi.org/10.1016/j.ijhydene.2016.04.041.
[42] K. Qian, A. Kumar, H. Zhang, D. Bellmer, R. Huhnke, Recent advances in utilization of biochar, Renewable Sustainable Energy Rev. 42 (2015) 1055–1064, https://doi.org/10.1016/j.rser.2014.10.074.
[43] P.S. Thue, E.C. Lima, J.M. Sieliechi, C. Saucier, S.L.P. Dias, J.C.P. Vaghetti, F.S. Rodembusch, F.A. Pavan, Effects of first-row transition metals and impregnation ratios on the physicochemical properties of microwave-assisted activated carbons from wood biomass, J. Colloid Interface Sci. 486 (2017) 163–175, https://doi.org/10.1016/j.jcis.2016.09.070.
[44] C. Kalinke, P.R. Oliveira, G.A. Oliveira, A.S. Mangrich, L.H. Marcolino-Junior, M.F. Bergamini, Activated biochar: Preparation, characterization and electroanalytical application in an alternative strategy of nickel determination, Anal. Chim. Acta 983 (2017) 103–111, https://doi.org/10.1016/j.aca.2017.06.025.
[45] B. Chen, Z. Chen, S. Lv, A novel magnetic biochar efficiently sorbs organic pollutants and phosphate, Bioresour. Technol. 102 (2011) 716–723, https://doi.org/10.1016/j.biortech.2010.08.067.
[46] S. Lowell, J.E. Shields, M.A. Thomas, M. Thommes, Characterization of porous solids and powders: surface area, pore size, and density, Springer Science Business Media, LLC, New York (2004), https://doi.org/10.5860/choice.42-5288.
[47] S.J. Gregg, K.S.W. Sing, Adsorption, Surface Area and Porosity, Second, Academic Press Inc, London, 1982, https://doi.org/10.1149/1.2426447.
[48] A. Kumar, H.M. Jena, Applied Surface Science High surface area microporous activated carbons prepared from Fox nut (Euryale ferox) shell by zinc chloride activation, Appl. Surf. Sci. 356 (2015) 753–761, https://doi.org/10.1016/j.apsusc.2015.08.074.
[49] W. Li, K. Yang, J. Peng, L. Zhang, S. Guo, H. Xia, Effects of carbonization temperatures on characteristics of porosity in coconut shell chars and activated carbons derived from carbonized coconut shell chars, Ind. Crops Prod. 28 (2008) 190–198, https://doi.org/10.1016/j.indcrop.2008.02.012.
[50] J.R. Sohn, S.H. Lee, Acidic properties of nickel sulfate supported on TiO2-ZrO 2 and catalytic activity for acid catalysis, Appl. Catal. A Gen. 266 (2004) 89–97, https://doi.org/10.1016/j.apcata.2004.01.034.
[51] A. Satsuma, A. Hattori, K. Mizutani, A. Furuta, A. Miyamoto, T. Hattori, Y. Murakami, Surface active sites of vanadium pentoxide-tungsten trioxide catalysts, J. Phys. Chem. 92 (1988) 6052–6058, https://doi.org/10.1021/j100332a042.
[52] L. Xie, Q. Gao, C. Wu, J. Hu, Rapid hydrothermal synthesis of bimetal cobalt nickel phosphate molecular sieve CoVSB-1 and its ammonia gas adsorption property, Microporous Mesoporous Mater. 86 (2005) 323–328, https://doi.org/10.1016/j.micromeso.2005.07.044.
[53] S.R. Pillai, S.H. Sonawane, S.P. Gumfekar, P.L. Suryawanshi, M. Ashokkumar, I. Potoroko, Continuous flow synthesis of nanostructured bimetallic Pt-Mo/C catalysts in milli-channel reactor for PEM fuel cell application, Mater. Chem. Phys. 237 (2019) 121854, , https://doi.org/10.1016/j.matchemphys.2019.121854.
[54] L. Qiang, L. Wen-zhi, Z. Dong, Z. Xi-feng, Analytical pyrolysis–gas chromatography/mass spectrometry (Py–GC/MS) of sawdust with Al/SBA-15 catalysts, J. Anal. Appl. Pyrolysis 84 (2009) 131–138, https://doi.org/10.1016/j.jaap.2009.01.002.
[55] Q. Lu, W.-M. Xiong, W.-Z. Li, Q.-X. Guo, X.-F. Zhu, Catalytic pyrolysis of cellulose with sulfated metal oxides: a promising method for obtaining high yield of light furan compounds, Bioresour. Technol. 100 (2009) 4871–4876, https://doi.org/10.1016/j.biortech.2009.04.068.
[56] M.A. Balubaid, W. Ahmad, Octane rating of gasoline and octane booster additives, Petroleum Science and Technology (2015), https://doi.org/10.1080/10916466.2015.1050506.

JECE 2020-Santi

ORIGINALITY REPORT

23%	16%	21%	5%
SIMILARITY INDEX	INTERNET SOURCES	PUBLICATIONS	STUDENT PAPERS

PRIMARY SOURCES

1	Li, W.. "Effects of carbonization temperatures on characteristics of porosity in coconut shell chars and activated carbons derived from carbonized coconut shell chars", Industrial Crops & Products, 200809 Publication	1%
2	Submitted to Universitas Jambi Student Paper	1%
3	asianpubs.org Internet Source	1%
4	www.mdpi.com Internet Source	1%
5	www.tandfonline.com Internet Source	1%
6	coek.info Internet Source	1%
7	Apaydın-Varol, Esin, and Yeliz Erülken. "A study on the porosity development for biomass based carbonaceous materials",	1%

Journal of the Taiwan Institute of Chemical Engineers, 2015.
Publication

---

8 Wang, Yangang, Yuting Chen, Mingcui Yao, Hengfei Qin, Shifei Kang, Xi Li, Yuanhui Zuo, Xiaodong Zhang, and Li-Feng Cui. "Simple synthesis of mesoporous FeNi/graphitic carbon nanocomposite catalysts and study on their activities in catalytic cracking of toluene", Materials Chemistry and Physics, 2015. <1 %
Publication

---

9 vdocuments.mx <1 %
Internet Source

---

10 P. González-García. "Activated carbon from lignocellulosics precursors: A review of the synthesis methods, characterization techniques and applications", Renewable and Sustainable Energy Reviews, 2018 <1 %
Publication

---

11 Adistya Husna, Fitria Febrianti, Habibie Syah, Rabiatul Pangaribuan, Tia Surbakti, Junifa Sihombing, Ahmad Pulungan. "Conversion of Cellulose From Palm Oil Middle Waste (Elaeis Guineensis) Into Bio-Oil Products As Alternative Fuel", Egyptian Journal of Chemistry, 2022 <1 %
Publication

---

www.semanticscholar.org

12	Internet Source	<1%
13	Gurwinder Singh, Kripal S. Lakhi, In Young Kim, Sungho Kim, Prashant Srivastava, Ravi Naidu, Ajayan Vinu. " Highly Efficient Method for the Synthesis of Activated Mesoporous Biocarbons with Extremely High Surface Area for High-Pressure CO Adsorption ", ACS Applied Materials & Interfaces, 2017 Publication	<1%
14	repositorio.pucrs.br Internet Source	<1%
15	www.sciencegate.app Internet Source	<1%
16	ibl.kb.nl Internet Source	<1%
17	María Luz Nieva Lobos, Juan Manuel Sieben, Vanina Comignani, Marta Duarte, María Alicia Volpe, Elizabeth Laura Moyano. "Biochar from pyrolysis of cellulose: An alternative catalyst support for the electro-oxidation of methanol", International Journal of Hydrogen Energy, 2016 Publication	<1%
18	rasayanjournal.co.in Internet Source	<1%

19	Cristiane Kalinke, Paulo Roberto Oliveira, Geovane Arruda Oliveira, Antonio Sálvio Mangrich et al. "Activated biochar: Preparation, characterization and electroanalytical application in an alternative strategy of nickel determination", Analytica Chimica Acta, 2017 Publication	<1 %
20	pubs.rsc.org Internet Source	<1 %
21	vdoc.pub Internet Source	<1 %
22	Gesha Desy Alisha, Wega Trisunaryanti, Akhmad Syoufian, Savitri Larasati. "Synthesis of high stability Mo/SiO2 catalyst utilizing Parangtritis beach sand for hydrocracking waste palm oil into biofuel", Biomass Conversion and Biorefinery, 2021 Publication	<1 %
23	Wega Trisunaryanti, Savitri Larasati, Syaiful Bahri, Yatim lailun Ni'mah et al. "Performance Comparison of Ni-Fe Loaded on NH2-Functionalized Mesoporous Silica and Beach Sand in the Hydrotreatment of Waste Palm Cooking Oil", Journal of Environmental Chemical Engineering, 2020 Publication	<1 %

24	A. Venegas-Gómez, M. Gómez-Corzo, A. Macías-García, J.P. Carrasco-Amador. "Charcoal obtained from cherry stones in different carbonization atmospheres", Journal of Environmental Chemical Engineering, 2019 Publication	<1 %
25	pub.epsilon.slu.se Internet Source	<1 %
26	"Handbook of Porous Solids", Wiley, 2002 Publication	<1 %
27	N. Soltani, A. Bahrami, M.I. Pech-Canul, L.A. González. "Review on the physicochemical treatments of rice husk for production of advanced materials", Chemical Engineering Journal, 2015 Publication	<1 %
28	mafiadoc.com Internet Source	<1 %
29	Jacek Grams, Michał Niewiadomski, Agnieszka M. Ruppert, Witold Kwapiński. "Catalytic performance of a Ni catalyst supported on CeO2, ZrO2 and CeO2–ZrO2 in the upgrading of cellulose fast pyrolysis vapors", Comptes Rendus Chimie, 2015 Publication	<1 %
30	www.freepatentsonline.com Internet Source	<1 %

31	Submitted to 9561 Student Paper	<1 %
32	www.scribd.com Internet Source	<1 %
33	epdf.tips Internet Source	<1 %
34	Triyono, W. Trisunaryanti, A. Syoufian, A. P. Wibawa, E. Suarsih, D.A. Fatmawati. "PREPARATION OF Co, Ni, AND Zn-BASED CATALYST SUPPORTED ON MESOPOROUS CARBON FOR HYDROCRACKING OF PYROLYZED α-CELLULOSE", Rasayan Journal of chemistry, 2021 Publication	<1 %
35	jyx.jyu.fi Internet Source	<1 %
36	Qiang Lu, Zhe Tang, Ying Zhang, Xi-feng Zhu. "Catalytic Upgrading of Biomass Fast Pyrolysis Vapors with Pd/SBA-15 Catalysts", Industrial & Engineering Chemistry Research, 2010 Publication	<1 %
37	Yifei Yang, Litao Jia, Yan Meng, Bo Hou, Debao Li, Yuhan Sun. "Fischer–Tropsch Synthesis over Ordered Mesoporous Carbon Supported Cobalt Catalysts: The Role of Amount of Carbon Precursor in Catalytic Performance", Catalysis Letters, 2011	<1 %

Publication

38	emitter.pens.ac.id Internet Source	<1%
39	Gesha Desy Alisha, Wega Trisunaryanti, Akhmad Syoufian. "Hydrocracking of Waste Palm Cooking Oil into Hydrocarbon Compounds over Mo Catalyst Impregnated on SBA-15", Silicon, 2021 Publication	<1%
40	Guangjian Zeng, Long Huang, Qiang Huang, Meiying Liu et al. "Rapid synthesis of MoS 2 - PDA-Ag nanocomposites as heterogeneous catalysts and antimicrobial agents via microwave irradiation", Applied Surface Science, 2018 Publication	<1%
41	Rong Zhu, Qiongfen Yu, Ming Li, Hong Zhao, Shaoxuan Jin, Yaowei Huang, Jie Fan, Jie Chen. "Analysis of factors influencing pore structure development of agricultural and forestry waste-derived activated carbon for adsorption application in gas and liquid phases: A review", Journal of Environmental Chemical Engineering, 2021 Publication	<1%
42	Submitted to Universiti Teknologi MARA Student Paper	<1%

43	Submitted to Udayana University Student Paper	<1 %
44	Yangyu Liu, Arman Peyravi, Zaher Hashisho, Shuilin Zheng, Zhiming Sun, Xiao Chen, Yuping Tong, Yongxing Hao, Jiuyue Wang. "Experimental and simulation investigation of water vapor adsorption on mesoporous MCM-41 derived from natural Opoka", Separation and Purification Technology, 2023 Publication	<1 %
45	aaqr.org Internet Source	<1 %
46	psasir.upm.edu.my Internet Source	<1 %
47	Antonakou, E.V., K.G. Kalogiannis, S.D. Stefanidis, S.A. Karakoulia, K.S. Triantafyllidis, A.A. Lappas, and D.S. Achilias. "Catalytic and thermal pyrolysis of polycarbonate in a fixed-bed reactor: The effect of catalysts on products yields and composition", Polymer Degradation and Stability, 2014. Publication	<1 %
48	Hasan Sayğılı, Gülbahar Akkaya Sayğılı. "Optimized preparation for bimodal porous carbon from lentil processing waste by microwave-assisted K2CO3 activation: Spectroscopic characterization and dye	<1 %

decolorization activity", Journal of Cleaner Production, 2019
Publication

49	Jie Yang, Limin Yue, Xin Hu, Linlin Wang, Yongle Zhao, Youyou Lin, Yan Sun, Herbert DaCosta, Liping Guo. " Efficient CO Capture by Porous Carbons Derived from Coconut Shell ", Energy & Fuels, 2017 Publication	<1 %
50	Komvokis, V.G., S. Karakoulia, E.F. Iliopoulou, M.C. Papapetrou, I.A. Vasalos, A.A. Lappas, and K.S. Triantafyllidis. "Upgrading of Fischerâ€“Tropsch synthesis bio-waxes via catalytic cracking: Effect of acidity, porosity and metal modification of zeolitic and mesoporous aluminosilicate catalysts", Catalysis Today, 2012. Publication	<1 %
51	Nguyen-Thanh, D.. "Metal-loaded carbonaceous adsorbents templated from porous clay heterostructures", Microporous and Mesoporous Materials, 20060620 Publication	<1 %
52	backend.orbit.dtu.dk Internet Source	<1 %
53	www.jmaterenvironsci.com Internet Source	<1 %

54	Didem Özmen, Naime Aslı Sezgi, Suna Balcı. "Synthesis of boron nitride nanotubes from ammonia and a powder mixture of boron and iron oxide", Chemical Engineering Journal, 2013 Publication	<1 %
55	Huaiyan Sun, Xinyu Jin, Feng Jiang, Ruifeng Zhang. " Immobilization of horseradish peroxidase on ZnO nanowires/macroporous SiO composites for the complete decolorization of anthraquinone dyes ", Biotechnology and Applied Biochemistry, 2018 Publication	<1 %
56	Jing Li, Jianjun Dai, Guangqing Liu, Hedong Zhang, Zuopeng Gao, Jie Fu, Yanfeng He, Yan Huang. "Biochar from microwave pyrolysis of biomass: A review", Biomass and Bioenergy, 2016 Publication	<1 %
57	Qiangu Yan, Caixia Wan, Jian Liu, Jinsen Gao, Fei Yu, Jilei Zhang, Zhiyong Cai. "Iron nanoparticles in situ encapsulated in biochar-based carbon as an effective catalyst for the conversion of biomass-derived syngas to liquid hydrocarbons", Green Chemistry, 2013 Publication	<1 %
58	S.D. Stefanidis, K.G. Kalogiannis, E.F. Iliopoulou, A.A. Lappas, P.A. Pilavachi. "In-situ	<1 %

upgrading of biomass pyrolysis vapors: Catalyst screening on a fixed bed reactor", Bioresource Technology, 2011
Publication

59	Yunpu Wang, Qi Yang, Linyao Ke, Yujie Peng, Yuhuan Liu, Qiuhao Wu, Xiaojie Tian, Leilei Dai, Roger Ruan, Li Jiang. "Review on the catalytic pyrolysis of waste oil for the production of renewable hydrocarbon fuels", Fuel, 2021 Publication	<1 %
60	aip.scitation.org Internet Source	<1 %
61	patents.google.com Internet Source	<1 %
62	studentsrepo.um.edu.my Internet Source	<1 %
63	www.hoghimwei.com Internet Source	<1 %
64	Girisuta, Buana, Konstantinos G. Kalogiannis, Karla Dussan, James J. Leahy, Michael H.B. Hayes, Stylianos D. Stefanidis, Chrysa M. Michailof, and Angelos A. Lappas. "An integrated process for the production of platform chemicals and diesel miscible fuels by acid-catalyzed hydrolysis and downstream upgrading of the acid hydrolysis residues with	<1 %

thermal and catalytic pyrolysis", Bioresource Technology, 2012.
Publication

65 ir.gig.ac.cn:8080 <1%
Internet Source

66 Bin Cao, Zhen Xia, Shuang Wang, Abd El-Fatah Abomohra et al. "A study on catalytic co-pyrolysis of cellulose with seaweeds polysaccharides over ZSM-5: Towards high-quality biofuel production", Journal of Analytical and Applied Pyrolysis, 2018 <1%
Publication

67 Bingbing Qiu, Chenhao Yang, Qianni Shao, Ya Liu, Huaqiang Chu. "Recent advances on industrial solid waste catalysts for improving the quality of bio-oil from biomass catalytic cracking: A review", Fuel, 2022 <1%
Publication

68 Collard, François-Xavier, Ammar Bensakhria, Martin Drobek, Ghislaine Volle, and Joël Blin. "Influence of impregnated iron and nickel on the pyrolysis of cellulose", Biomass and Bioenergy, 2015. <1%
Publication

69 Gęsikiewicz-Puchalska, A., M. Zgrzebnicki, B. Michalkiewicz, U. Narkiewicz, A.W. Morawski, and R.J. Wrobel. "Improvement of CO2 uptake of activated carbons by treatment with <1%

mineral acids", Chemical Engineering Journal, 2017.
Publication

---

70 M. L. Ang, U. Oemar, E. T. Saw, L. Mo, Y. Kathiraser, B. H. Chia, S. Kawi. " Highly Active Ni/ Na/CeO Catalyst for the Water–Gas Shift Reaction: Effect of Sodium on Methane Suppression ", ACS Catalysis, 2014 <1 %
Publication

---

71 Parisa Moradi, Maryam Hajjami, Bahman Tahmasbi. "Fabricated copper catalyst on biochar nanoparticles for the synthesis of tetrazoles as antimicrobial agents", Polyhedron, 2020 <1 %
Publication

---

72 Paulo André Cremonez, Joel Gustavo Teleken, Thompson Weiser Meier. "Potential of Green Diesel To Complement the Brazilian Energy Production: A Review", Energy & Fuels, 2020 <1 %
Publication

---

73 Ronghua Li, Wen Liang, Jim J. Wang, Lewis A. Gaston et al. "Facilitative capture of As(V), Pb(II) and methylene blue from aqueous solutions with MgO hybrid sponge-like carbonaceous composite derived from sugarcane leafy trash", Journal of Environmental Management, 2018 <1 %
Publication

74	Tao, Bing, and Ashleigh J. Fletcher. "Metaldehyde removal from aqueous solution by adsorption and ion exchange mechanisms onto activated carbon and polymeric sorbents", Journal of Hazardous Materials, 2013. Publication	<1 %
75	eprints.undip.ac.id Internet Source	<1 %
76	peralta18.files.wordpress.com Internet Source	<1 %
77	s-space.snu.ac.kr Internet Source	<1 %
78	scholarbank.nus.edu.sg Internet Source	<1 %
79	smujo.id Internet Source	<1 %
80	sphinxsai.com Internet Source	<1 %
81	www.cellulosechemtechnol.ro Internet Source	<1 %
82	A Aho. "Catalytic pyrolysis of woody biomass", Biofuels, 03/2010 Publication	<1 %

83	Andreas Schmidt, Andrij Dreger. "Recent Advances in the Chemistry of Pyrazoles. Part 2. Reactions and N-Heterocyclic Carbenes of Pyrazole", Current Organic Chemistry, 2011 Publication	<1 %
84	Baofeng Zhao, Xiaodong Zhang, Anzhuang Xu, Weijing Ding, Laizhi Sun, Lei Chen, Haibin Guan, Shuangxia Yang, Weihong Zhou. "A study of the in-situ CO 2 removal pyrolysis of Chinese herb residue for syngas production", Science of The Total Environment, 2018 Publication	<1 %
85	Cheah, Willie, Soraya Hosseini, Moonis Ali Khan, T.G. Chuah, and Thomas S.Y. Choong. "Acid modified carbon coated monolith for methyl orange adsorption", Chemical Engineering Journal, 2013. Publication	<1 %
86	Jain, Akshay, Rajasekhar Balasubramanian, and M.P. Srinivasan. "Hydrothermal conversion of biomass waste to activated carbon with high porosity: A review", Chemical Engineering Journal, 2016. Publication	<1 %
87	Jenjira Phuriragpitikhon, Pramila Ghimire, Mietek Jaroniec. "Tannin-derived micro-mesoporous carbons prepared by one-step	<1 %

activation with potassium oxalate and CO2", Journal of Colloid and Interface Science, 2020
Publication

88	Jong Rack Sohn, Jun Seob Lim. "Catalytic Activities of Al2O3-promoted NiSO4/TiO2 for Acid Catalysis", Catalysis Letters, 2006 Publication	<1 %
89	d-nb.info Internet Source	<1 %
90	depositonce.tu-berlin.de Internet Source	<1 %
91	digital.csic.es Internet Source	<1 %
92	digitalcommons.usu.edu Internet Source	<1 %
93	e-spacio.uned.es Internet Source	<1 %
94	opus.bath.ac.uk Internet Source	<1 %
95	pt.scribd.com Internet Source	<1 %
96	repositorio.ufmg.br Internet Source	<1 %
97	tel.archives-ouvertes.fr Internet Source	<1 %

98	tsukuba.repo.nii.ac.jp Internet Source	<1 %
99	" Effect of V O Modification in V O /TiO -ZrO Catalysts on Their Surface Properties and Catalytic Activities for Acid Catalysis ", Bulletin of the Korean Chemical Society, 2007 Publication	<1 %
100	Iliopoulou, E.F., S.D. Stefanidis, K.G. Kalogiannis, A. Delimitis, A.A. Lappas, and K.S. Triantafyllidis. "Catalytic upgrading of biomass pyrolysis vapors using transition metal-modified ZSM-5 zeolite", Applied Catalysis B Environmental, 2012. Publication	<1 %
101	Gazali Tanimu, Ahmed T. Al-Qathmi, Abdullah M. Aitani, Sachio Asaoka, Ziyauddin S. Qureshi, Hassan Alasiri. " Oxidative Dehydrogenation of -Butenes to 1,3-Butadiene over Ni-BiO Metal Oxides Supported on Mesoporous SBA-15 ", Industrial & Engineering Chemistry Research, 2023 Publication	<1 %
102	Moonjung Kim, Suk Hoo Yoon, Eunsoo Choi, Bogim Gil. "Comparison of the adsorbent performance between rice hull ash and rice hull silica gel according to their structural	<1 %

differences", LWT - Food Science and Technology, 2008
Publication

103 Rungnapa Kaewmeesri, Jeeranan Nonkumwong, Worapon Kiatkittipong, Navadol Laosiripojana, Kajornsak Faungnawakij. "Deoxygenations of palm oil-derived methyl esters over mono- and bimetallic NiCo catalysts", Journal of Environmental Chemical Engineering, 2021 <1%
Publication

Exclude quotes	On	Exclude matches	< 5 words
Exclude bibliography	On		